REPORT DOCUMENTATION PAGE

Form Approved OMB NO. 0704-0188

1. REPORT DATE (DD-MM-YYYY)	2. REPORT TYPE	3. DATES COVERED (From - To)
21-05-2015	Final Report	10-Oct-2011 - 9-Jan-2015

4. TITLE AND SUBTITLE

Final Report: Understanding the Scientific Basis of Electrocaloric Effect In Defects Modified Ferroelectric Polymers

5a. CONTRACT NUMBER
W911NF-11-1-0534

5b. GRANT NUMBER

5c. PROGRAM ELEMENT NUMBER
611102

6. AUTHORS
Lei Zhu, Qiming Zhang

5d. PROJECT NUMBER

5e. TASK NUMBER

5f. WORK UNIT NUMBER

7. PERFORMING ORGANIZATION NAMES AND ADDRESSES
Pennsylvania State University
Office of Sponsored Programs
110 Technology Center Building
University Park, PA 16802 -7000

8. PERFORMING ORGANIZATION REPORT NUMBER

9. SPONSORING/MONITORING AGENCY NAME(S) AND ADDRESS (ES)

U.S. Army Research Office
P.O. Box 12211
Research Triangle Park, NC 27709-2211

10. SPONSOR/MONITOR'S ACRONYM(S)
ARO

11. SPONSOR/MONITOR'S REPORT NUMBER(S)
60345-MS.21

12. DISTRIBUTION AVAILIBILITY STATEMENT

Approved for Public Release; Distribution Unlimited

13. SUPPLEMENTARY NOTES

The views, opinions and/or findings contained in this report are those of the author(s) and should not contrued as an official Department of the Army position, policy or decision, unless so designated by other documentation.

14. ABSTRACT

Materials with large electrocaloric effect (ECE) is attractive for Army and DoD applications such as for the thermal management of soldier's in battle field, cooling of electronic systems, and mobile cooling units with high cooling power, compact size, and high efficiency. Recent experiments have demonstrated large ECE in the relaxor ferroelectrics (defects modified ferroelectrics) over broad temperatures. Ferroelectrics provide a strong coupling of polarization to the applied field (easy to induce a large polarization) and the defects structures can be employed to facially tailor the "randomness" of dipoles to achieve large ECE. This program develops fundamental

15. SUBJECT TERMS

electrocaloric effect (ECE), relaxor ferroelectrics, multicomponent relaxor, nano-composite

16. SECURITY CLASSIFICATION OF:			17. LIMITATION OF ABSTRACT	15. NUMBER OF PAGES	19a. NAME OF RESPONSIBLE PERSON
a. REPORT	b. ABSTRACT	c. THIS PAGE			Qiming Zhang
UU	UU	UU	UU		19b. TELEPHONE NUMBER 814-863-8994

Report Title

Final Report: Understanding the Scientific Basis of Electrocaloric Effect In Defects Modified Ferroelectric Polymers

ABSTRACT

Materials with large electrocaloric effect (ECE) is attractive for Army and DoD applications such as for the thermal management of soldier's in battle field, cooling of electronic systems, and mobile cooling units with high cooling power, compact size, and high efficiency. Recent experiments have demonstrated large ECE in the relaxor ferroelectrics (defects modified ferroelectrics) over broad temperatures. Ferroelectrics provide a strong coupling of polarization to the applied field (easy to induce a large polarization) and the defects structures can be employed to facially tailor the "randomness" of dipoles to achieve large ECE. This program develops fundamental understanding of large ECE in the relaxor ferroelectrics.Through experimental study and thermodynamics analysis, we intend to address these questions: (a) what are the polarization responses in these complex and highly coupled polar-materials that control the entropy change in the materials and (b) how to influence these polarization responses and consequently ECE via various molecular and nanocomposite approaches

Enter List of papers submitted or published that acknowledge ARO support from the start of the project to the date of this printing. List the papers, including journal references, in the following categories:

(a) Papers published in peer-reviewed journals (N/A for none)

Received		Paper
02/22/2013	7.00	Xiangzhong Chen, Xinyu Li, Xiaoshi Qian, Shan Wu, Shengguo Lu, Haiming Gu, Minren Lin, Qundong Shen, Qiming Zhang. A polymer blend approach to tailor the ferroelectric responses in P(VDF-TrFE) based copolymers, Polymer, (04 2013): 0. doi:
03/03/2014	13.00	Xiao-Shi Qian, Hui-Jian Ye, Ying-Tang Zhang, Haiming Gu, Xinyu Li, C. A. Randall, Q. M. Zhang. Giant Electrocaloric Response Over A Broad Temperature Range in Modified BaTiO, Advanced Functional Materials, (03 2014): 1300. doi: 10.1002/adfm.201302386
05/18/2012	2.00	Run Su, Jung-Kai Tseng, Mao-Sheng Lu, Minren Lin, Qiang Fu, Lei Zhu. Ferroelectric behavior in the high temperature paraelectric phase in a poly(vinylidene fluoride-co-trifluoroethylene) random copolymer, Polymer, (02 2012): 728. doi: 10.1016/j.polymer.2012.01.001
05/20/2015	19.00	Xiao-Shi Qian, Dae-Yong Jeong, Hui-Jian Ye, Shujun Zhang, Yue Zhou, Wen-Zhu Shao, Liang Zhen, Q. M. Zhang. Giant electrocaloric effect in BaZr0. 2Ti0. 8O3 thick film, Applied Physics Letters, (10 2014): 152908. doi:
05/29/2012	3.00	Xiang-zhong Chen, Xiao-shi Qian, Xinyu Li, S.G. Lu, Hai-ming Gu, Minren Lin, Qun-dong Shen, Q. M. Zhang. Enhanced electrocaloric effect in poly(vinylidene ?uoride- trifluoroethylene)-based terpolymer/copolymer blends, Applied Physics Letters, (05 2012): 222902. doi:
07/10/2014	12.00	Xiao-Shi Qian, Hui-Jian Ye, Ying-Tang Zhang, Haiming Gu, Xinyu Li, C. A. Randall, Q. M. Zhang. Electrocaloric Materials: Giant Electrocaloric Response Over A Broad Temperature Range in Modified BaTiO, Advanced Functional Materials, (03 2014): 1336. doi: 10.1002/adfm.201470060
07/22/2013	8.00	Xinyu Li, Sheng-Gou Lu, Xiang-Zhong Chen, Haiming Gu, Xiaoshi Qian, Qiming Zhang. Electrocaloric and Pyroelectric Materials, J Materials Chemistry A, (01 2013): 23. doi:
07/22/2013	9.00	Xiang-Zhong Chen, Xinyu Li, Xiao-Shi Qian, ShanWu, Sheng-Guo Lu, Hai-Ming Gu, Minren Lin, Qun-Dong Shen, Qiming Zhang. A polymer blend approach to tailor the ferroelectric responses in P (VDFeTrFE)based copolymers, Polymer, (04 2013): 2373. doi:
08/23/2012	4.00	Z. K. Liu, Xinyu Li, Q. M. Zhang. Maximizing the number of coexisting phases near invariant critical points for giant electrocaloric and electromechanical responses in ferroelectrics, Applied Physics Letters, (08 2012): 0. doi: 10.1063/1.4747275
11/26/2012	5.00	Xinyu Li, Sheng-Guo Lu, Xiang-Zhong Chen, Haiming Gu, Xiao-shi Qian, Q. M. Zhang. Pyroelectric and electrocaloric materials, Journal of Materials Chemistry C, (01 2013): 0. doi: 10.1039/c2tc00283c
11/26/2012	6.00	Lianyun Yang, Xinyu Li, Elshad Allahyarov, Philip L. Taylor, Q. M. Zhang, Lei Zhu. Novel Polymer Ferroelectric Behaviors via Crystal Isomorphism and the Nanoconfinement Effect, Polymer, (02 2013): 0. doi:

TOTAL: 11

Number of Papers published in peer-reviewed journals:

(b) Papers published in non-peer-reviewed journals (N/A for none)

Received Paper

TOTAL:

Number of Papers published in non peer-reviewed journals:

(c) Presentations

Number of Presentations: 1.00

Non Peer-Reviewed Conference Proceeding publications (other than abstracts):

Received Paper

TOTAL:

Number of Non Peer-Reviewed Conference Proceeding publications (other than abstracts):

Peer-Reviewed Conference Proceeding publications (other than abstracts):

Received Paper

TOTAL:

Number of Peer-Reviewed Conference Proceeding publications (other than abstracts):

(d) Manuscripts

Received		Paper
05/20/2015	20.00	Xiaoshi Qian, Tiannan Yang, Tian Zhang, Long-Qing Chen, Q. M. Zhang. Anomalous Electrocaloric Effect, ADVANCED MATERIALS (05 2015)
07/22/2013	10.00	Xiang-Zhong Chen, Xinyu Li, Xiao-Shi Qian, Minren Lin, Shan Wu, Qun-Dong Shen, Q. M. Zhang . A nanocomposite approach to tailor electrocaloric effect in ferroelectric polymer, Polymer (05 2013)
07/22/2013	11.00	Xiao-Shi Qian, Hui-Jian Ye, Ying-Tang Zhang, Haiming Gu, Xinyu Li, C. A. Randall, Q. M. Zhang*. Giant Electrocaloric Response Over A Broad Temperature Range in Modified BaTiO3 Ceramics, Advanced Functional Materials (07 2013)
09/29/2014	16.00	Hui-Jian Ye, , Xiao-Shi Qian, , Dae-Yong Jeong, , Shujun Zhang, , Yue Zhou, , Wen-Zhu Shao, , Liang Zhen, , Q. M. Zhang. Giant electrocaloric effect in BaZr0.2Ti0.8O3 thick film, Applied Physics Letters (08 2014)
09/29/2014	17.00	S. Pamir Alpay, , Joseph Mantese, , Susan Trolier-McKinstry, , Qiming Zhang, , Roger W. Whatmore,. Next Generation Electrocaloric and Pyroelectric Materials for Solid State Electrothermal Interconversion, MRS Bulletin (09 2014)
09/29/2014	18.00	Hui-Jian Ye, , Dae-Yong Jeong, , Jinhuang Lu, , Xiao-Shi Qian, , Haiming Gu, , Shujun Zhang, , Wen-Zhu Shao, , Liang Zhen , Q. M. Zhang. The dielectric and polarization properties of BaZr0.2Ti0.8O3 bulk ceramic and thick film with sintering aids, IEEE Transactions on Dielectrics and Electrical Insulation (09 2014)
TOTAL:		**6**

Number of Manuscripts:

Books

Received		Book
TOTAL:		

Received	Book Chapter

07/10/2014 15.00 . Chapt 5. Electrocaloric Polymers , : , ( )

TOTAL: **1**

Patents Submitted

Patents Awarded

Awards

Xiaoshi Qian has received Dr. Nirmal K. Bose Dissertation Excellence Award in May 2014 from the Electrical Engineering Department of Penn State.

Graduate Students

NAME	PERCENT_SUPPORTED	Discipline
Xiaoshi Qian	0.10	
FTE Equivalent:	**0.10**	
Total Number:	**1**	

Names of Post Doctorates

NAME	PERCENT_SUPPORTED
Minren Lin	0.10
FTE Equivalent:	**0.10**
Total Number:	**1**

Names of Faculty Supported

NAME	PERCENT_SUPPORTED
FTE Equivalent:	
Total Number:	

Names of Under Graduate students supported

NAME	PERCENT_SUPPORTED
FTE Equivalent:	
Total Number:	

Student Metrics

This section only applies to graduating undergraduates supported by this agreement in this reporting period

The number of undergraduates funded by this agreement who graduated during this period: 0.00

The number of undergraduates funded by this agreement who graduated during this period with a degree in science, mathematics, engineering, or technology fields:..... 0.00

The number of undergraduates funded by your agreement who graduated during this period and will continue to pursue a graduate or Ph.D. degree in science, mathematics, engineering, or technology fields:..... 0.00

Number of graduating undergraduates who achieved a 3.5 GPA to 4.0 (4.0 max scale):..... 0.00

Number of graduating undergraduates funded by a DoD funded Center of Excellence grant for Education, Research and Engineering:..... 0.00

The number of undergraduates funded by your agreement who graduated during this period and intend to work for the Department of Defense 0.00

The number of undergraduates funded by your agreement who graduated during this period and will receive scholarships or fellowships for further studies in science, mathematics, engineering or technology fields: 0.00

Names of Personnel receiving masters degrees

NAME

Total Number:

Names of personnel receiving PHDs

NAME

Total Number:

Names of other research staff

NAME PERCENT_SUPPORTED

FTE Equivalent:

Total Number:

Sub Contractors (DD882)

Inventions (DD882)

Scientific Progress

Please see attachement

Technology Transfer

Final Report

Understanding the Scientific Basis of Electrocaloric Effect in Defects Modified Ferroelectrics

ARO: W911NF-11-1-0534

Program Manager: Chakrapani Varanasi

Period covered: Oct 10, 2011 to December 31, 2014

Submitted by

Qiming Zhang

The Pennsylvania State University, University Park, PA 16802

e-mail: qxz1@psu.edu; ph: 814-863-8994

Lei Zhu

Case Western Reserve University, OH

December 19, 2014

A brief summary on the major accomplishments during the past three years:

Materials with large electrocaloric effect (ECE) is attractive for Army and DoD applications such as for the thermal management of soldier's in battle field, cooling of electronic systems, and mobile cooling units with high cooling power, compact size, and high efficiency. Recent experiments have demonstrated large ECE in the relaxor ferroelectrics (defects modified ferroelectrics) over broad temperatures. Ferroelectrics provide a strong coupling of polarization to the applied field (easy to induce a large polarization) and the defects structures can be employed to facially tailor the "randomness" of dipoles to achieve large ECE. This program develops fundamental understanding of large ECE in the relaxor ferroelectrics. Through experimental study and thermodynamics analysis, we intend to address these questions: (a) what are the polarization responses in these complex and highly coupled polar-materials that control the entropy change in the materials and (b) how to influence these polarization responses and consequently ECE via various molecular and nanocomposite approaches.

During the first year of this program, **(I)** We have investigated the three different types of relaxor ferroelectric polymers, which exhibit different ECEs, and the study reveals that the different nano-defects structures have profound effect on polarization responses at high electric fields (> 100 MV/m) and consequently the ECE.

(II) We derived general thermodynamic conditions in order to maximize the ECE in given ferroelectric materials, i.e., searching for and operating the material near an invariant critical point (ICP) where the energy barriers among the coexisting phases become very small. Moreover, by tailoring the constraints to maximize the number of coexisting phases near ICPs, large ECE (as well as electromechanical response) may be realized. We show that *by operating PMN-PT near the ICP, the ECE is more than double that of pure PMN*. We also extended the research in the first year on the invariant critical point (ICP), which when combined with defects modifications to ferroelectric $BaTiO_3$, leading to giant ECE in $Ba(TiZr)O_3$ ferroelectric ceramics. These studies reveal the promise of working with multi-phase and multi- component defects (especially through the interfacial effects) modified ferroelectrics in achieving a large polarization response and also giant ECE.

(III) We investigated the effect of nanoparticles such as ZrO_2 on the polarization responses and consequently the ECE and it was found that even with small amount of ZrO_2 nanoparticles (~ 1 Vol%) can cause a large change in the polarization and ECE (enhancement) of the P(VDF-TrFE-CFE) relaxor ferroelectric polymers.

(IV) We investigated a multicomponent relaxor nano-composite in which the P(VDF-TrFE-CFE) is blended with a normal ferroelectric P(VDF-TrFE). It was observed that the addition of small amount of P(VDF-TrFE) (<10 wt% or vol%) can lead to an enhanced relaxor polarization response and consequently a 50% enhancement in the ECE. The microstructural studies reveal that it is the nanoscale coupling of the small amount of P(VDF-TrFE) copolymer with the defects structure of the terpolymer that converts the P(VDF-TrFE) into the relaxor, which enhances the relaxor polarization response and ECE. These studies show the promise of working with multil-phase and multi-component defects modified ferroelectrics in achieving a large ECE.

(V) More excitingly, by tuning the defects coupling in the blends of normal ferroelectric P(VDF-TrFE) and relaxor terpolymer P(VDF-TrFE-CFE), we discovered an anomalous ECE. That is, the dielectric material will cool under an electric pulse with no subsequent heat generated. (In normal ECE, applying an electric field to a dielectric material will cause heating and removing

the field will cause cooling.). The discovery of the anomalous ECE opens up a totally new ECE research direction as well as new applications.

I. Understand the polarization responses in the two classes of relaxor ferroelectric (RFE) polymers

1.1 Double Hysteresis Loop behavior in P(VDF-TrFE)-based Terpolymers

After annealing the uniaxially stretched P(VDF-TrFE-CFE) terpolymer film at 70 °C for 1 h, the sample contains 100% RFE phase. Temperature dependent hysteresis loops at various poling frequencies are shown in Fig. 1. At -25 °C, double loops with significant hysteresis and remanent polarization are observed with decreasing the poling frequency to below 100 Hz. At 1000 Hz, the dipoles cannot catch up with the electric field and much less hysteresis is seen. The large hysteresis can be attributed to the larger domain size in the RFE phase when the temperature is low enough. When increasing the temperature to 0 and 25 °C, the hysteresis in D-E loops continuously decrease due to a continuous decrease in the domain size and an increase in the interchain distance. At 25 °C, a significant amount of RFE phase should transform into the PE phase. Therefore, the remanent polarization reduces to nearly zero and typical DHLs are observed. We speculate that the double hysteresis is caused by the electric field-induced RFE/PE→FE phase transition upon poling and the FE→RFE/PE phase transition upon removing the field, because the FE phase is indeed observed after mechanical stretching. Currently, we do not have a direct proof for the FE phase during in-situ electric poling process. In the future, we will use time-resolved polarized FTIR to investigate dipole flipping and phase transitions in uniaxially stretched P(VDF-TrFE-CFE) terpolymer films. At 50 °C (above the T_C at 22 °C), the sample becomes 100% PE phase. As a result, narrow hysteresis loops are observed at 1000 Hz, similar to laterally expanded P(VDF-TrFE) crystals, namely, e-beam crosslinked P(VDF-TrFE) copolymers and P(VDF-TrFE)-based terpolymers the D-E loops at 1000 Hz for the P(VDF-TrFE) film in the PE phase. With decreasing the frequency, a sense of double hysteresis is observed at high fields. This again can be attributed to some FE domain formation within the PE matrix at high enough electric poling fields. After annealing the uniaxially stretched P(VDF-TrFE-CFE) film in the PE phase at 70 °C, the film quality decreases, resulting in a significant reduction in breakdown strength. Therefore, it is very difficult for us to obtain a full set of D-E loops at 1 Hz poling frequency at 70 °C.

The origin for the DHLs observed for P(VDF-TrFE-CFE) terpolymers is explained in the bottom panel of Fig. 2. In the first step, pre-expansion of the interchain distance in PVDF crystals by TrFE via repeating unit isomorphism is important, namely, $l2>l1$ where $l1$ and $l2$ are interchain distances in PVDF and P(VDF-TrFE) crystals, respectively. This first step expansion of interchain distance makes it possible to further incorporate the even larger third comonomer, such as VC, CFE, CDFE, and CTFE, into the isomorphic crystalline structure. A good example for this effect is to compare P(VDF-CTFE) with P(VDF-TrFE-CTFE). For P(VDF-CTFE), the CTFE repeating units are too large to be effectively incorporated in a PVDF crystal. As a result, most CTFE units are rejected out of the PVDF crystal and no RFE behavior can be observed in P(VDF-CTFE). However, CTFE can be effectively incorporated into a P(VDF-TrFE) crystal, leading to an RFE behavior. The incorporation of the even larger third comonomer further expands the interchain distance, namely, $l3>l2$, where $l3$ is the interchain distance of the terpolymer crystal. Note that HFP cannot be incorporated into P(VDF-TrFE) to form the RFE phase because HFP unit is too large. Meanwhile, these larger comonomers can effectively pin the P(VDF-TrFE) chains, if they are randomly distributed along the chain. For example,

for the P(VDF-TrFE-CFE) 59.2/33.6/7.2 terpolymer, on average two neighboring CFE units can pin about 14 VDF/TrFE repeating units. This pinning will allow the in-between P(VDF-TrFE) chains to freely rotate because they do not tightly touch one another. However, these CFE units can only provide temporary physical pinning. When the poling electrical field becomes high enough, dipoles start to switch because the CFE unit also has a dipole moment. Consequently, the high electric field will generate FE domains within the RFE matrix. However, these FE domains should be weaker than those formed by mechanical stretching because they can transform back to the RFE phase after decreasing the poling field. We speculate that the electric field-induced FE domains in the terpolymer may be large enough so that significant hysteresis is observed during the RFE↔FE transitions.

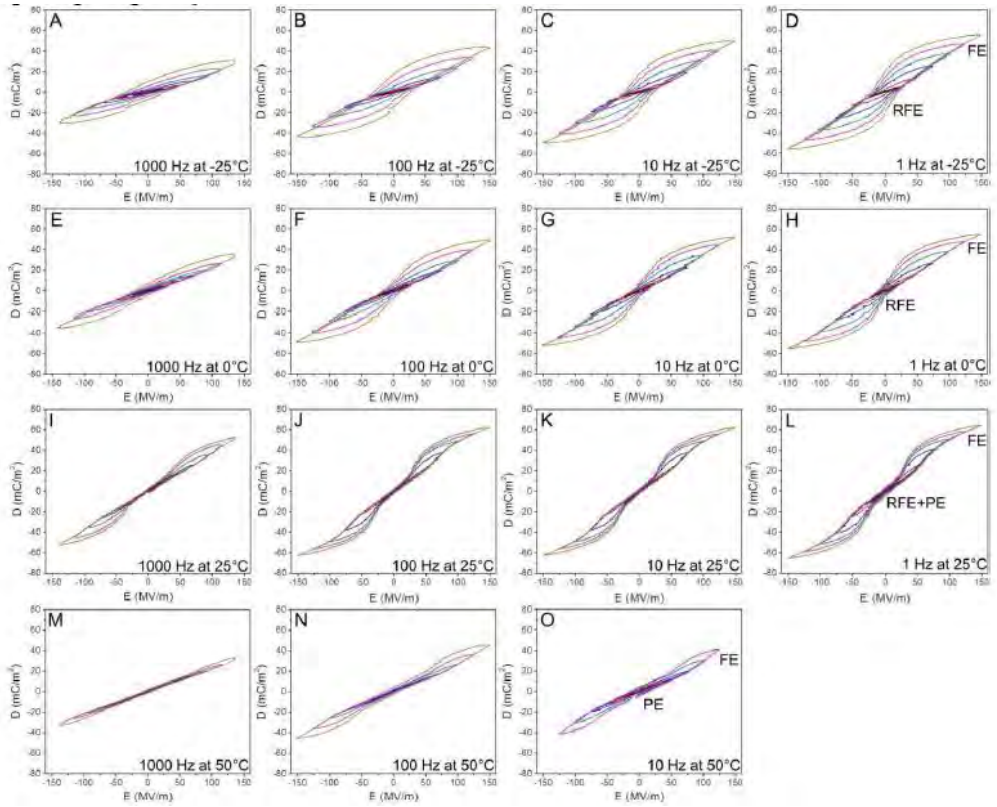

Fig. 1. Bipolar hysteresis loops for the 70 °C-annealed uniaxially stretched P(VDF-TrFE-CFE) terpolymer film at (A-D) -25 °C, (E-G) 0 °C, (I-L) 25 °C, and (M-O) 50 °C, respectively. The poling frequency varies from left to right: (A, E, I, M) 1000 Hz, (B, F, J, N) 100 Hz, (C, G, K, O) 10 Hz, and (D, H, L) 1 Hz. Note that at 50 °C, the 70 °C-annealed film is easy to breakdown and thus no results for 1 Hz bipolar poling can be obtained. All poling field (triangular waveform) starts at 25 MV/m with a stepwise increase of 25 MV/m except for those at 1000 Hz.

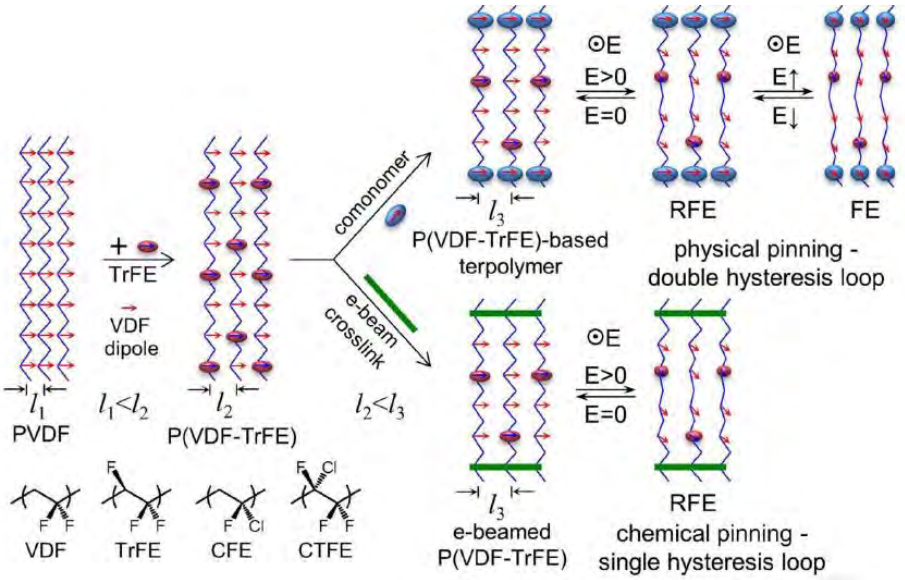

Fig. 2. Schematic representations of physical (temporary) and chemical (permanent) pinning in laterally expanded P(VDF-TrFE) crystals, namely, P(VDF-TrFE)-based terpolymers and e-beam crosslinked P(VDF-TrFE) copolymers.

From the above discussion, it would be better to permanently pin P(VDF-TrFE) chains in the crystal in order to avoid the hysteresis during the RFE↔FE transitions. One effective way is to chemically crosslink the P(VDF-TrFE) crystal with an optimized crosslinking density (see the bottom panel in Fig. 2). Nonetheless, there has not been any effective ways to crosslink polymer crystals via chemical reactions because polymer crystals do not allow penetration of crosslinking agents such as molecular radicals into them. Instead, ionizing radiations, such as e-beam, γ-ray, and proton radiation, have been used to crosslink PVDF and PVDF-based copolymer crystals. Intriguingly, only P(VDF-TrFE) crystals are found to be susceptible to ionizing radiation and the interchain distance gradually increases with increasing the irradiation dose. PVDF and other PVDF- based copolymer crystals do not show similar changes in the crystalline phase upon ionizing radiation. This must be attributed to the special reactivity of TrFE upon ionizing radiations. For example, upon e-beam irradiation the TrFE units can transform into the >CH-CF3 groups, as evidenced by high temperature (170 °C) solid-state 19F NMR, although the detailed transformation mechanism is still unclear. We consider that the P(VDF-TrFE) crystals must be internally crosslinked. These internal chemical crosslinks not only expand the interchain distance, but also permanently pin the P(VDF-TrFE) chains in between. As a result, free dipole rotation, nanodomains and thus narrow hysteresis loops will be achieved.

1.2 Narrow Hysteresis Loop Behavior in E-beam Irradiated P(VDF-TrFE) Copolymers

Temperature dependent ferroelectric property of the e-beam irradiated (60 Mrad) uniaxially stretched P(VDF-TrFE) 50/50 film is studied by D-E loop measurements, and results are shown in Fig. 3. At -25 °C, the D-E loops are relatively opened and this can be attributed to the slightly increased domain size at such a low temperature. With increasing the temperature, the hysteresis in D-E loops gradually decreases and the most narrow hysteresis loops are observed at 25 °C. when the temperature increases to 50 °C, the D-E loops start to open up again, especially at 1 Hz. Finally, the hysteresis loops substantially open up for 1 Hz at 75 °C. The opened loops at high temperatures and low frequencies can be attributed to enhanced ion migrational loss and/or

dc conduction in the sample. For all these temperatures, the Dmax slightly increases with decreasing the poling frequency; however, the loop shape does not change much except for 1 Hz at 75 °C.

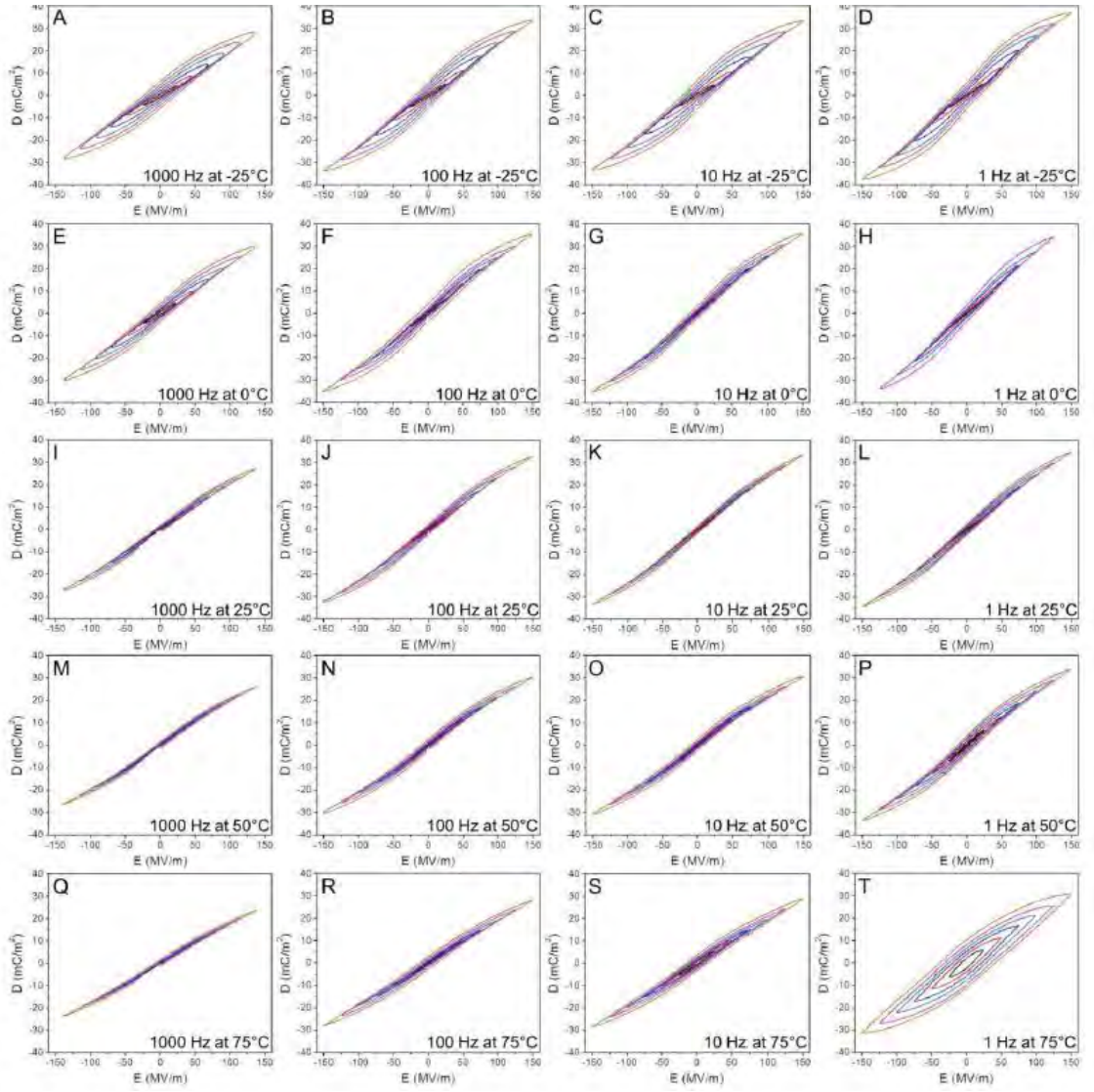

Fig. 3. Bipolar hysteresis loops for the e-beam irradiated (60 Mrad) uniaxially stretched P(VDF- TrFE) 50/50 film (draw ratio = 400%) at different temperatures: (A-D) -25 °C, (E-H) 0 °C, (I-L) 25 °C, (M-P) 50 °C, and (Q-T) 75 °C. The poling frequencies decrease from left to right: (A, E, I, M, Q) 1000, (B, F, J, N, R) 100, (C, G, K, O, S) 10, and (D, H, L, P, T) 1 Hz, respectively. All poling field (a triangular waveform) starts at 25 MV/m with a stepwise increase of 25 MV/m except those at 1000 Hz.

This temperature dependent RFE behavior can be explained using the schematic representation in the bottom panel of Fig. 2. First, we hypothesize that the inclusion of TrFE is critical for e-beam induced crosslinking inside the crystals, because PVDF and its other copolymers do not show the RFE behavior even after e-beam irradiation. After high energy e-beam irradiation, the crystal is internally crosslinked and this is important for the appearance of the RFE behavior. When the crosslinking density is low (e.g., 20 Mrad at 70 °C), the sample is still ferroelectric, with a decreased TC. When the crosslinking density increases to a critical

value (e.g., with 40 and 60 Mrad irradiation at 70 °C), the true RFE behavior can be achieved without any observation of TC. The crosslinking of both amorphous and crystalline phases has prevented detailed structure analysis of what has happened in the crystal. However, we speculate that the crosslinks inside the crystal permanently pin P(VDF-TrFE) chains with suitable segmental lengths, resulting in nanodomains (see the bottom panel of Fig. 2). Therefore, the pinned P(VDF-TrFE) chains in between behave like torsional springs and the conventional FE-to-PE Curie transition is effectively prohibited. Meanwhile, the interchain distance is also enlarged, as evidenced from the WAXD study. With applying an external electric field, the dipoles in the pinned P(VDF-TrFE) chains can more or less freely rotate. Due to the nature of permanent pinning and enlarged interchain distance to reduce the dipole-dipole interactions, the FE domains must be small both perpendicular and parallel to the chain direction. It is these nanodomains with freely rotatable main-chain dipoles that result in a true RFE behavior (i.e., narrow single hysteresis loops) in e-beam irradiated P(VDF-TrFE). Because of the lack of effective experimental methods to determine the size and shape of ferroelectric domains at the nanoscale, we resort to computer simulation to "visualize" these nanodomains later. Finally, when the crosslinking density is too high in the crystal, P(VDF-TrFE) chains will be permanently locked in and the dipole switching will be lost as observed in previous reports. Although the chemical pinning effectively eliminated the TC in the sample, the size of these nanodomains may still be temperature dependent. At low temperatures (e.g., -25 °C), the nanodomains appear larger and thus the D-E loops open up (see Figs. 3A-D). As the size of nanodomains gradually decreases, narrow hysteresis loops are observed (e.g., at 0-50 °C). With further increasing the temperature, the mobility of P(VDF-TrFE) chains in the pinned crystals becomes so high that both impurity ion loss and dc conduction significantly increase, as we discussed above. As a result, the D-E loops will eventually open up at high temperatures and low frequencies.

II. Multi-phased relaxor nanomaterial systems:

2.1 Operating the material near an invariant critical point (ICP)

Besides the pure polymers, multi-phase or multi-component material systems such as polymer blends and nanocomposites provide an effective means to study the polarization response and ECE in these defects modified ferroelectric polymers.

One critical issue in developing relaxor ferroelectrics for Army and DoD thermal management (cooling) applications is how to design and tailor ferroelectric materials to achieve high electrocaloric (EC) response. Recently, it has been demonstrated that by operating near phase transitions, giant EC response can be realized. Moreover, it has also been showed that the giant electromechanical (EM) response in $Pb(Mg_{1/3}Nb_{2/3})O_3$-$PbTiO_3$ (PMN-PT) is a manifestation of two-phase critical points that define a line of critical end points (LCEP) in the electric-field–temperature–composition ($E-T-x_{PT}$) phase diagram of this

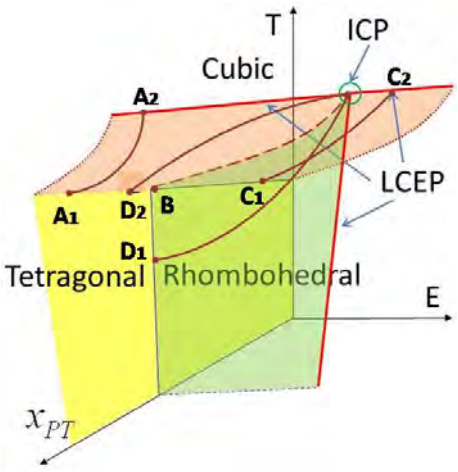

Fig. 4. Schematic of an $E-T-x$ three dimensional phase diagram with an ICP (point C), using PMN-PT as an example with major phases presented (the labeling of the phases refers to the zero-electric field phases).

system. Near the LCEP, the energy barrier for the phase transition is lowered markedly, leading to the giant EM response. In this program, we show that not all the points along a LCEP are equal and much larger EC or EM can be realized by maximizing the number of coexisting phases near invariant critical points (ICP).

As an example, **Fig. 4** presents schematically a phase diagram of $E-T-x_{PT}$ (using PMN-PT relaxor ceramics as an example) in which multiple phases can co-exist and energy barriers for the phase transformations near ICP are low, thus leading to large EC and EM responses.

For a ferroelectric material, the combined first and second laws of thermodynamics can be written as follows

$$dU = TdS + V\sum_{i,j}\left(-\sigma_{ij}\right)d\varepsilon_{ij} + V\sum_i E_i dD_i + \sum_i \mu_i dN_i, \qquad (1)$$

where U is the internal energy with its natural variables being entropy (S), strains (ε_{ij}), electric displacements (D_i), chemical components (N_i), and their conjugate quantities being temperature (T), 6 stresses (σ_{ij}), 3 electric field components (E_i), and the chemical potential (μ_i). V is the volume. The Gibbs phase rule of the system is written as

$$\nu = c + 1 + 6 + 3 - p = c + 10 - p, \qquad (2)$$

where p denotes the number of phases co-existing at equilibrium due to the Gibbs-Duhem relation, and c is the number of components. The critical point, i.e. the limit of stability of a homogeneous single phase system, is defined when the following when,

$$\left(\frac{\partial Y^a}{\partial X^a}\right)_{X^c Y^{b\neq a,c}} = 0, \qquad (3)$$

where X^a and Y^a represent each natural variable and its conjugate variable, respectively, and $Y^{b\neq a,c}$ includes all other potentials, except Y^a and Y^c. For a homogeneous single phase system, Eq. 3 contains c + 9 equations except Y^c as X^c is kept constant, and consequently the degree of freedom ν of the system at a critical point becomes zero. We thus name the critical point in this c + 10 dimensional space of potentials an invariant critical point (ICP). Let n_S represent the number of potentials fixed, the maximum number of phases can co-exist before an ICP is reached is thus

$$p_{max} = c + 9 - n_s. \qquad (4)$$

In a two-dimensional phase diagram, for example the temperature and electric field ($T-E$) phase diagram of PMN-PT under the ambient pressure and given composition ($c = 2$ and $n_s = 9$ for 6 stress, 2 electric field components, and given composition, noting that all phases have the same composition during ferroelectric transitions), becomes $p_{max} = 2 + 9 - 9 = 2$, i.e. two phases. Furthermore, there exists an ICP in the $E-T-x_{PT}$ three-dimensional phase diagram (see **Fig. 4**) that involves three phases at the two ends of LCEPs with $n_s = 8$ (six stress and two electric field components), and $p_{max} = 3$ with $c = 2$ (see **Fig. 4** near ICP).

These three-phase ICPs will have potential to reach larger EM and EC responses than those along the LCEPs due to one more phase introduced. Any two-phase equilibrium among the three phases before the ICP is reached can be described by the generalized Clausius-Clapeyron equation,

$$\left(\frac{\partial Y^a}{\partial Y^b}\right) = -\frac{\Delta X^b}{\Delta X^a}, \qquad (5)$$

with ΔX being the difference between two coexisting phases. For the case $Y^a = T$ and $Y^b = -\sigma_{ij}$, of $\Delta X^a = \Delta S$ and $\Delta X^b = \Delta\varepsilon_{ij}$. Thus, a larger ΔS at an ICP may also lead to a larger strain change, resulting in larger electromechanical response than those along the two-phase LCEP away from ICP. Hence, these ICPs provide a new avenue in designing ferroelectric materials with large EC and EM responses.

The analysis can be expanded to phase diagrams with higher than three dimensions where more than three phases can coexist, having potential to reach even higher EC and EM responses.

For example, $E - T - \sigma_1 - \sigma_2 - x_2 - x_3$ of a ternary system with $n_s = 6$ (4 stress and 2 electric field components fixed), $p_{max} = 6$, as illustrated in **Fig. 5** using $PbMgO_3$-$PbNbO_3$-$PbTiO_3$ (PM-PN-PT) as an example. For $(PM_y\text{-}PN_{1-y})_{1-x}\text{-}PT_x$ thin films near the morphotropic phase boundary (x~0.3, y~1/3), multiple phases (p_{max} = 6) could coexist, including rhombohedral (Rh), two monoclinic (M), orthorhombic (O), tetragonal (T), cubic, for example with local polarization directions randomly distributed along symmetry allowed directions. Using the entropy for a ferroelectric phase, along with the concept of phase mixture where a disordered paraelectric phase is considered as a random mixture of various dipole orientations, the entropy of a dipolar system can be written as

$$S_{dip} = -\sum_i \frac{k}{v_i} c_i \ln(c_i/\Omega_i), \quad (6)$$

where k is the Boltzmann constant, c_i is the volume fraction of i^{th} phase, Ω_i the number of polar-states in the i^{th} phase, and v_i the average volume associated with each dipolar unit in the i^{th} phase (smallest unit of v_i is given by the volume per molecular unit). With Rh (Ω =8), O (Ω =12), T (Ω =6), and two monoclinic phases M_C and M_B (Ω =8 for both of them) in a PM-PN-PT thin film near an ICP along MPB and, for the simplicity, also assume c_i =1/5 and $v_i = v_0$ for all the phases. Eq. 6 shows that the entropy becomes $S_{dip} = 3.71k/v_0$, which is much larger compared with a composition near pure PMN (pure Rh phase, Ω =8), which has a $S_{dip} = 2.08k/v_0$. If a high field can lead to a total saturation of polarization (Ω =1), leading to $S_{dip}(E_{max})$=0. Thus, a much higher ΔS in EC response near ICP can be achieved. For the example here, ΔS_{dip}(near ICP)/ΔS_{dip}(Rh) ~ 1.79, an enhancement of about 80%.

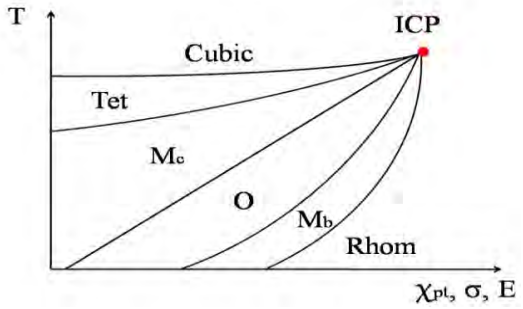

Fig. 5. Schematic of an $E - T - \sigma_1 - \sigma_2 - x_{PT} - x_{PM}$ multidimensional dimensional phase diagram with an ICP, using PM-PN-PT as an example with all the phases reported presented (the labeling of the phases refers to the zero-electric field phases). For simplicity, x, σ, and E are drawn on the same axis.

The theoretical result here is consistent with the available experimental data. For example, for $PMN_{1-x}\text{-}PT_x$ thin films at compositions near pure PMN (e.g., x<0.15) ΔS was reported in the range of 1.7 to 3.6 J $mol^{-1}K^{-1}$, while for $PMN_{1-x}\text{-}PT_x$ thin films at composition near MPB (x ~ 0.3), a much higher ΔS, from 3.7 to 8.7 J $mol^{-1}K^{-1}$ can be induced. Here on average the experimentally observed enhancement ΔS_{dip}(near ICP)/ΔS_{dip}(Rh) is 2.3.

These results demonstrate the potential of working with multi-phase and multi-component material systems at near ICPs in enhancing the ECE.

2.2 Realizing the invariant critical point (ICP) in and defects modifications to $BaTiO_3$ -- giant electrocaloric response and relaxor behavior in modified $BaTiO_3$ (BT) ceramics

As a lead-free ferroelectric material which is environmentally friendly and is in fact the most widely used ferroelectric material, ECE in BT has been studied quite extensively in the past several years by many groups and in various forms including thin films, bulk ceramics (including thick films multilayer ceramic capacitors (MLCC)), and single crystals. Large ΔT and ΔS have been reported in BT ceramics at temperatures near the ferroelectric-paraelectric (FE-PE) transition.

It is noted that for BT, besides the high temperature FE-PE transition (the transition temperature T_{FE-PE}> 100 ^{o}C) between the tetragonal ferroelectric (Tet) and cubic paraelectric phase, also exhibits an orthorhombic (O) and a rhombohedral (Rhom) phases as illustrated in **Fig. 6**(a). As ECE is directly related to the entropy change of an insulation dielectric under the change of the applied electric field, a dielectric with a polar phase which contains a large number of polar-states with similar energy levels can be induced under a reasonable electric field from a non-polar phase (for example, below the dielectric breakdown field of the dielectric) has the potential of achieving giant ΔT and ΔS. Moreover, a giant ECE can be induced under a low electric field ΔE if the energy barriers for switching between the polar-states are vanishingly small. For pure BT at the FE-PE transition, the FE tetragonal phase (Tet) has six equivalent polar-states and a large dielectric constant at FE-PE transition causes a large $\Delta T/\Delta E$ at temperatures right above the FE-PE transition, as has been observed in single crystal BT. On the other hand, as suggested by Liu et al., by operating near an invariant critical point (ICP) at which all the four phases (paraelectric cubic, Tet, O, and Rhom) can coexist, there is an increased number of available polar states (twenty-six states) that leads to a significant increase in the entropy of the non-polar phase, leading to giant ΔT and ΔS. Moreover, the near zero energy barriers near ICP imply a low field for inducing switching between these different states and hence a giant ECE can be induced under low electric fields.

It is well known and has been extensively studied that the temperature of the three phase

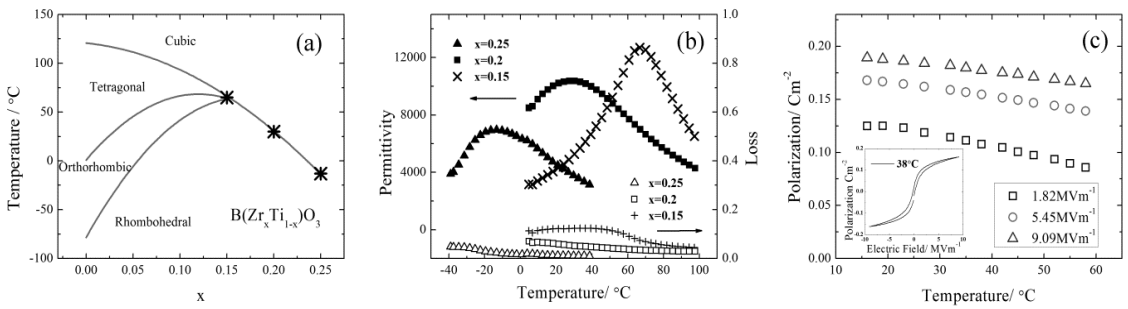

Fig. 6. (a) Phase diagram of $Ba(Zr_xTi_{1-x})O_3$ solid solution systems. Stars (*) are the dielectric constant maxima from this study. (b) Weak-field dielectric properties as functions of temperature for BZT(x=0.15, 0.2 and 0.25). (c) Polarization as a function of temperature for BZT(x=0.2) under different electric fields. The inset shows a polarization-electric field loop (P-E loop) for BZT(x=0.2) at 38°C.

transitions in BT can be easily moved by chemical modifications in the BT. As presented in **Fig. 6**(a), by working with a solid solution of $Ba(Zr_xTi_{1-x})O_3$, these three transitions will merge into an ICP at x~ 0.15, near which the four phases can coexist near room temperature. Here, we show that for BZT(x=0.2), a relaxor composition near ICP occurs and a giant ECE property exists, i.e., both a large ΔT and $\Delta T/\Delta E$ can be obtained near room temperature over a broad temperature range (from 25 to 50 oC) in bulk ceramic samples.

Fig. 6(b) presents the dielectric properties measured at 1 kHz of BZT ceramics at x=0.15, x=0.2, and x=0.25 compositions. The BZT(x=0.2) samples display a broad dielectric constant peak at 25 ^{o}C and relaxor dielectric response, consistent with earlier studies. The induced polarization P vs. temperature, obtained from the polarization hysteresis loops taken from

BZT(x=0.2) sample at different applied field amplitudes at 100 Hz and temperatures, is presented in **Fig. 6**(c). The induced polarization decreases with temperature continuously from 15 ^{o}C to 60 ^{o}C and does not exhibit any peak around 25 ^{o}C, consistent with the relaxor nature of the material. The dielectric peak of BZT(x=0.15) occurs at a temperature near 67 ^{o}C and peak is narrower compared with that of BZT(x=0.2). ECE results of the three BZT compositions were characterized and BZT(x=0.2) exhibits the highest EC response which also occurs near room temperature. BZT(x=0.15) displays a slightly reduced ECE which peaks at 67 ^{o}C, compared with BZT(x=0.2), but is higher than that of BZT(x=0.25).

The directly recorded ECE signal from BZT(x=0.2) (at 35 ^{o}C under a ΔE = 9.5 MVm^{-1}) is presented in **Fig. 7**(a), which shows the temperature rise and drop as the field is applied and removed from the ceramic sample. ΔS and ΔT from the temperature drop of the sample as the field is removed are presented in **Fig. 7**(b) for the BZT(x=0.2) at 35 ^{o}C under different ΔE. The data reveals that at ΔE = 14 MVm^{-1}, ΔT_c = - 4.5 K and ΔS = 8 Jkg^{-1}K^{-1} (Q = 2.5 Jg^{-1}) are obtained. Here ΔT_c is introduced to represent the temperature drop (cooling) of the sample as the field is reduced. As shown in **Fig. 7**(c), ΔT_c and ΔS do not show much change over a broad temperature range from 25 ^{o}C to 50 ^{o}C, and there is a very broad peak between 35 ^{o}C and 40 ^{o}C, higher than the broad dielectric constant peak temperature (=25 ^{o}C). For the bulk BZT(x=0.2) ceramic samples in the ECE study, the highest field that can be applied was 14 MVm^{-1}. To make a comparison with the results on BT thick films, we extrapolate the data in **Fig. 7**(b) to higher fields and it is deduced that ΔT_c = -7.1 K can be induced for BZT(x=0.2) ceramics under a field of 31 MVm^{-1}, which is more than two times lower than that required to induced the same ΔT (=80 MVm^{-1}) in the pure BT ceramics. This extrapolation is consistent with the induced polarization data of this BZT composition (assuming ΔT is proportional to the square of the polarization P) which can be measured up to 35 MVm^{-1}.The results are also consistent with prediction that giant ECE under low applied field can be achieved by operating near ICP to maximize the number of coexisting phases which have vanishing energy barriers to switch.

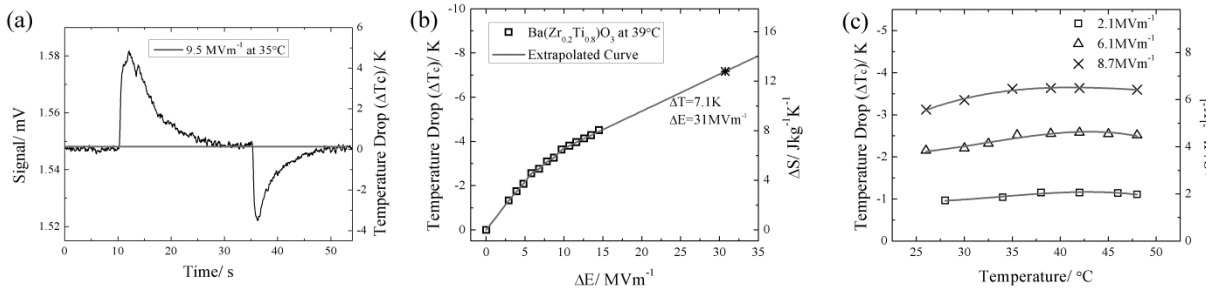

Fig. 7. (a) The directly recorded ECE signal for BZT(x=0.2) as the electric field was turning on and off, respectively. The data was measured under ΔE=9.5MVm^{-1} at 35°C. Solid line is drawn to show the ambient temperature reading. (b) EC induced temperature drop ΔT_C and isothermal temperature change ΔS as functions of ΔE for BZT(x=0.2) at 39°C. The data was extrapolated (solid curve) to estimate ΔT_C at higher electric fields. (c) ΔT_C and ΔS as functions of temperature for BZT(x=0.2) under different electric fields.

To measure quantitatively how effective an applied electric field ΔE in generating ECE in dielectrics, the ratio of $\Delta T_c/\Delta E$, $\Delta S/\Delta E$ (or $Q/\Delta E$, where $Q=T\Delta S$) have been introduced in early studies. These parameters are referred to as the electrocaloric coefficients. Analogous to many materials coefficients of ferroelectric materials such as the piezoelectric coefficients which change with the measuring field amplitude ΔE, the EC coefficients for BZT(x=0.2) also change with ΔE. Large EC coefficients ($|\Delta T_c/\Delta E| = 0.53\times10^{-6}$ KmV^{-1} and $\Delta S/\Delta E=0.93\times10^{-6}$ $Jmkg^{-1}K^{-1}V^{-1}$) are observed at ΔE = 2 MV/m and ΔT_c= -1.1 K. The coefficients decrease ($|\Delta T_c/\Delta E| = 0.31\times10^{-6}$ KmV^{-1} and $\Delta S/\Delta E=0.54\times10^{-6}$ $Jmkg^{-1}K^{-1}V^{-1}$) at higher ΔE=14.5 MVm^{-1} and ΔT_c= -4.5 K. In addition, the materials maintain the giant EC response over a broad temperature range, as indicated by **Fig. 7**(c).

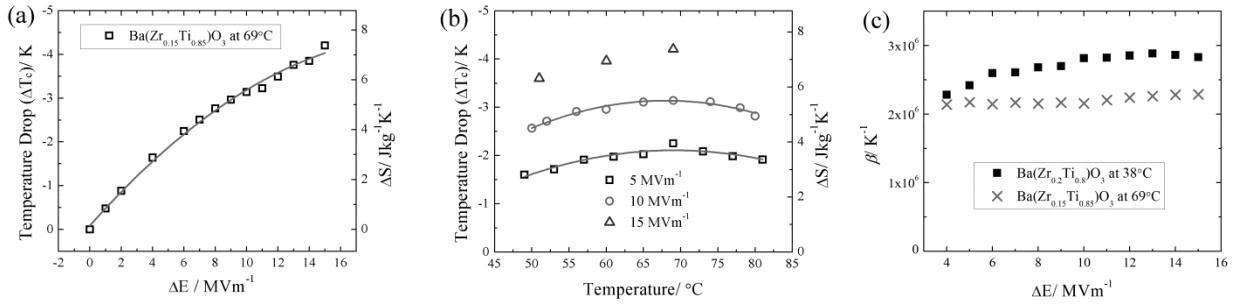

Fig.8. (a) Temperature drop as a function of applied field ΔE at 69°C for BZT(x=0.15). (b) Temperature drop ΔTc and isothermal entropy change ΔS as functions of temperatures under different electric fields. (c) β coefficient as a function of electric fields for BZT(x=0.15) and BZT(x=0.2) near the temperature of their respective ECE peaks.

Fig. 8(a) presents ΔT_c and ΔS of BZT(x=0.15) measured at 69 ^oC vs. ΔE and the data were taken from the temperature lowering of the sample as the field was removed. ΔT_c = -4.2 K and ΔS = 7.3 $Jkg^{-1}K^{-1}$ were induced under 15 MVm^{-1}. ΔT_c vs. temperature measured under different electric fields are shown in **Fig. 8**(b) and a slightly larger temperature variation is observed, when compared with the data in **Fig. 7**(c) for BZT(x=0.2). ΔT_c shows a broad peak near 69°C. The EC coefficients $|\Delta T_c/\Delta E|=0.48\times10^{-6}$ KmV^{-1} and $\Delta S/\Delta E=0.85\times10^{-6}$ $Jmkg^{-1}K^{-1}V^{-1}$ for BZT(x=0.15) under ΔE=1MVm^{-1}. The EC coefficients of BZT(x=0.15) is slightly lower than that of BZT(x=0.2). Similar to what is observed in BZT(x=0.2), the EC coefficient is reduced to $|\Delta T_c/\Delta E|=0.28\times10^{-6}$ K mV^{-1} and $\Delta S/\Delta E=0.5\times10^{-6}$ $Jmkg^{-1}K^{-1}V^{-1}$ under a higher electric field ΔE=15 MVm^{-1}. The study here as well as earlier studies all indicate that BZT(x=0.15) is where the three transitions merge (ICP) while BZT(x=0.2) exhibits "stronger" ferroelectric relaxor behavior compared with BZT(x=0.15). *The results suggest that it is the combination of ICP and ferroelectric relaxer behavior that leads to the giant ΔT_c and $\Delta T/\Delta E$ in the ceramic BZT near room temperature*. This is also consistent with the β coefficient, where β is defined from, $\Delta S = -\frac{1}{2}\beta P^2$, from BZT with different compositions. **Fig. 8**(c) shows that β for BZT(x=0.2) can be more than 25% higher than that of BZT(x=0.15). On the other hand, further increasing the

Fig. 9. Back-cover image of Adv. Funct. Mater. showing multi-phase (ICP) induced large ECE and potential for flat panel cooling devices.

composition to x=0.25 causes a reduction of ECE compared with that at x=0.2. This demonstration was back-cover highlighted by Advanced Functional Materials. (**Fig. 9**).

Table 1 compares the ECE from this study with the EC materials such as ceramics and polymers which have potential for practical cooling applications. The ECE data from single crystals and thin films (such as sub-micron thick films supported on foreign substrates) are also included, which may not be directly used for practical cooling devices. For practical applications, the temperature range in which a large ECE can be maintained is also critical. In the Table, T_{span} is introduced to measure this performance, which is the temperature span over which the ΔT_c maintains $0.9\times\Delta T_c$(maximum). As can be seen, the BZT developed here possesses a giant ECE, i.e., large ΔT_c, $\Delta T_c/\Delta E$, $\Delta S/\Delta E$ and T_{span}. The combination of these high performances indicate the potential of the material developed here for the ECE based cooling devices with high cooling power and efficiency.

Table 1. Comparison of EC properties of BZTs developed here with those in the literature.

Material	Form	T [°C]	ΔT_c [K]	ΔE [MVm^{-1}]	$\lvert\Delta T_c/\Delta E\rvert$ [10^{-6}KmV^{-1}]	$\Delta S/\Delta E$ [10^{-6}Jmkg^{-1}K^{-1}V]	T_{span}. [K]	Method	Reference
BZT(x=0.2) (high field)	Ceramic	39	4.5	14.5	0.31	0.54	>30	Direct	This work
BZT(x=0.2) (low field)	Ceramic	38	1.1	2.1	0.52	0.93	>30	Direct	This work
BZT(x=0.15)	Ceramic	69	4.2	15	0.28	0.5	>30	Direct	This work
BT	Ceramic	118	0.4	0.75	0.53		10	Direct	[17]
BT	Ceramic MLCC	80	7.1	80	0.09	0.12	80	DSC	[16]
BT	Ceramic MLCC	80	1.8	17.6	0.10			DSC	[8]
Doped BT	Ceramic MLCC	21	0.5	30	0.02	0.02	60	Direct	[32]
PMN	Ceramic	67	2.5	9	0.27			Direct	[10]
PMN-30PT	Ceramic	145	2.6	9	0.29			Direct	[10]
PLZT	Thin Film	45	40	120	0.33			Direct	[7]
Irradiated P(VDF-TrFE)	Polymer	33	35	180	0.13	0.63	50	Direct	[15]
P(VDF-TrFE-CFE)	Polymer	30	15.7	150	0.10	0.49	50	Direct	[33]
$Pb(Mg_{1/3}Nb_{2/3})_{0.75}Ti_{0.25}O_3$	Single Crystal	110	1.1	2.5	0.44			DSC	[5]

*ΔT_c is the temperature drop (cooling) in the ECE data. For the measurement methods, DSC refers to as the direct EC measurement using differential scanning calorimetry.

2.3 Developing modified BZT thick films and enhanced ECE of BZT thick films, due to stress-coupling from the substrate.

From the phase rule, in order to realize all 4 phase coexistence at ICP, additional variables are required besides the composition variable (x in BZT), temperature, and electric field. Moreover, the ferroelastic coupling in BZT may also be made use of to enhance the ECE, for example, by working with films on substrates. For practical cooling device applications, the BZT ceramic should be in multilayer form so that the applied field can be high even with a low applied voltage. Based on these considerations, in this option period, we have been working on BZT thick films (thickness ~ 10 μm) and as will be shown in the following, the BZT thick films exhibit even higher ECE than the bulk BZT ceramics (about 50% higher). This work is in close collaboration with and leverage the resources at *Penn State Center for Dielectric Studies (CDS)*, which is an NSF center and has extensive knowledge, facilities, and staffs in developing ceramic materials in various form.

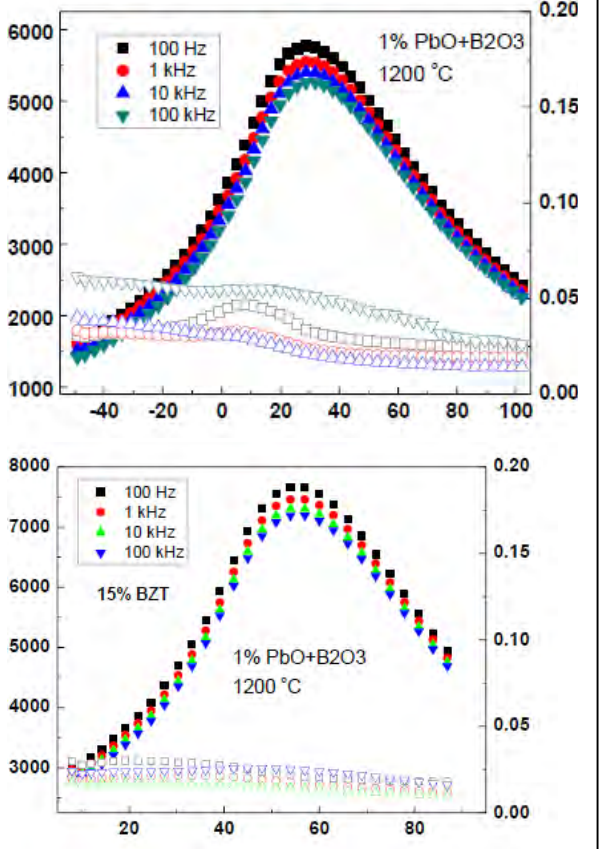

Fig. 10. Dielectric properties as functions of temperature for BZT x=0.2 (top) and x=0.15 (bottom) with 1 wt% PbO and B_2O_3 sintering aids. The ceramics were sintered at 1200 °C, a temperature suitable for fabricating multilayer ceramics and thick films with internal electrodes. The dielectric properties are very similar to that of bulk ceramics without sintering aids.

2.3.1 Sintering aids to lower the sintering temperature

The bulk BZT ceramics have been sintered at temperatures above 1350 °C (for example, BZT at x=0.2 was sintered at 1450 °C), which is too high for BZT thick films because of the need to co-fire the internal electrodes. In ceramics, it is well known that by employing small amount of appropriate sintering aids, the sintering temperature can be reduced while the other materials properties can be maintained. Hence, in collaboration with the CDS, we first studied the effects of different types of sintering aids to the sintering temperature and material properties of BZT bulk ceramics.

The bulk BZT samples were fabricated by a conventional solid-state reaction method. All the chemicals of barium carbonate ($BaCO_3$, 99.8 %, 1 micron), zirconium dioxide (ZrO_2, 99.5 %,

1 micron), and titanium dioxide (TiO_2, 99.5 %, 1 to 2 micron) were purchased from Alfa Aesar and used directly. Stoichiometric weights of all the powder were mixed with ethanol and milled by zirconia balls for 24 h. After the calcination performed at 1100 °C for 2 h, 0.5 mol.% MnO_2, 1 wt.% polyvinyl alcohol (PVA) binder solution and 1 to 3wt.% sinter aids (such as LiBiO2, PbO and B2O3) were added in and then pressed into disks under 10 MPa pressure using hydraulic press. Finally, the pellets were sintered from 1100 to 1200 °C in air for 1 h with a heating rate of 3 °C/min. The obtained samples were 10 mm in diameter and about 1 mm in thickness. The experimental results show that the sintering aids of PbO and B_2O_3 (1 wt%) can lower the sintering temperature to 1200 °C while the BZT ceramics maintain high dielectric and polarization responses. See Fig. 10.

2.3.2 Thick BZT film fabrication

Fig. 11 depicts the fabrication process for multilayer ceramics and CDS has maintained an in house facility which makes it easier to carry out the study. The multilayer of BZT film was prepared by the tape casting method. After the calcination of materials performed under 1100 °C for 2 h, the slurry with proper amount of vehicle A and B (polymer innovations) were used to fabricate thick films via tape casting. The BZT film around 15 µm was cast first onto the glass plate by a blade method. After the Pt electrode was printed on the BZT film, the multilayer bodies were hot pressed at 65 °C (5000 pounds) for 5 minutes. After the vacuum, the printed film is stacked layer by layer with precise alignment during the isostatic lamination (see Fig. 12). Then the multilayer films were cut in small size depending on the electrode size and allowed to burnout organics at 600℃ for 10 hours. Subsequently, the MLCCs are sintered to consolidate the layers of BZT films and Pt electrodes into the dense sample at 1200 °C in air for 1.5 h. Finally the metal terminations are applied to make the electrical connection to the internal electrodes exposed on the opposite ends.

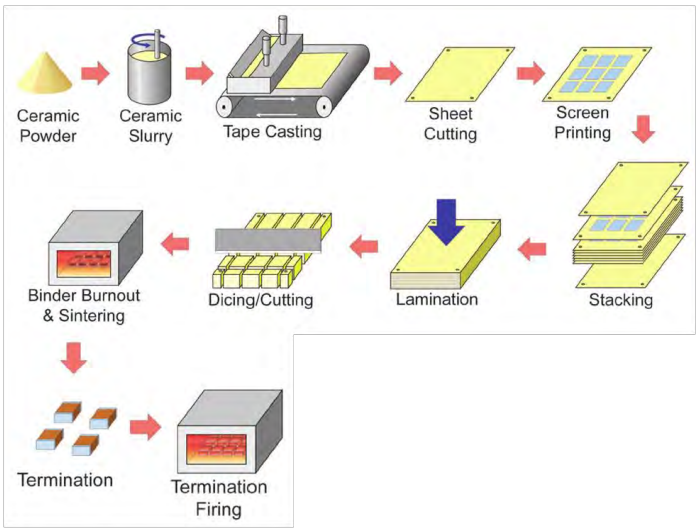

Fig. 11. Figure 6 A schematic of the MLCC fabrication process (M. J. Pan and C. A. Randall, IEEE Electrical Insulation Magazine, 2010, 26, 44)

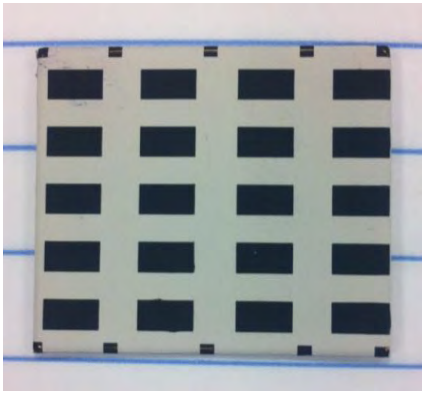

Fig. 12. An optic image of the MLCC tape fabricated.

2.3.3 Thick BZT film characterization

The cross-section SEM image of BZT x=0.2 multilayer films with two active layers is shown in **Fig. 13** (FEI NanoSEM 630 FESEM). Both of active layers are 12 µm thick, and the total thickness of this

lamination product is 560 μm. The dielectric properties are also shown in **Fig. 13**. The thick BZT films (12 mm thick) fabricated in MLCC process and configuration display nearly the same dielectric properties as that of the bulk (**Fig. 10**), indicating the high quality of the BZT MLCC. From earlier results, (Qian et al, Adv Func. Mater. 2014), the dielectric peak of bulk BZT ceramic at x=0.2 is around 29 °C. The peak of ceramic with sintering aids of PbO and B_2O_3 is about 20 °C, indicating a small shift of peak temperature after the addition of fluxes. The dielectric constant maintains high level (around 6500 at 20 °C) when the sintering temperature is lowered to 1200 °C from the 1450 °C without sintering aids. The dielectric loss is very low.

Polarization (P)-electric field (E) loops of BZT x=0.2 thick film obtained at 10 Hz with different electric field and test temperature are presented in **Fig. 14** (a) and (b). The polarization of BZT thick film reaches 0.20 C/m^2 at 20 MV/m and room temperature. The induced polarization decreases continuously with increasing temperature form 10 to 60 °C and exhibits no obvious peak in the test temperature range, which is consistent with the relaxor nature of the ceramic material. As shown in **Fig. 14**(c), BZT thick film exhibits slim polarization loops near the dielectric peak of15 °C.

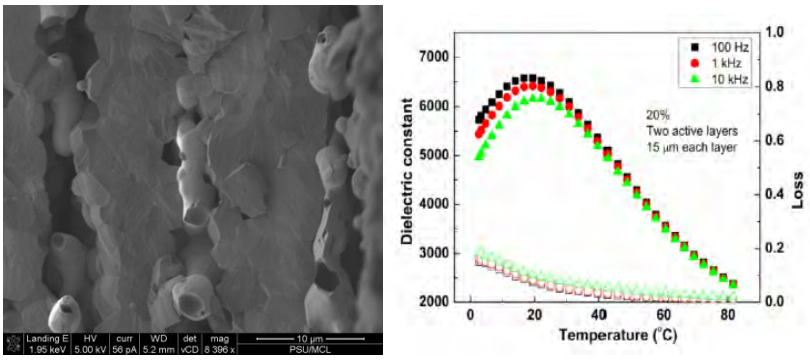

Fig. 13. (left) SEM image of cross section of the multilayer BZT x=0.2 and (right) the dielectric properties as function of temperature.

The heat Q generated and absorbed by ECE in BZT thick films were measured by the modified differential scanning calorimetry (DSC) (TA Q2000), from which ΔT and ΔS can be obtained. *Temperature drop of 6.3 ℃ and entropy change ΔS =11.0 Jkg^{-1}K^{-1} can be obtained under a field of 14.6 MV/m at 40 ℃, which is higher than that in bulk BZT (**Fig. 8**, ΔT = 4.5 °C under the similar field). Under 19.5 MV/m ΔT=7.0 ℃ is induced in the thick film.* The data are

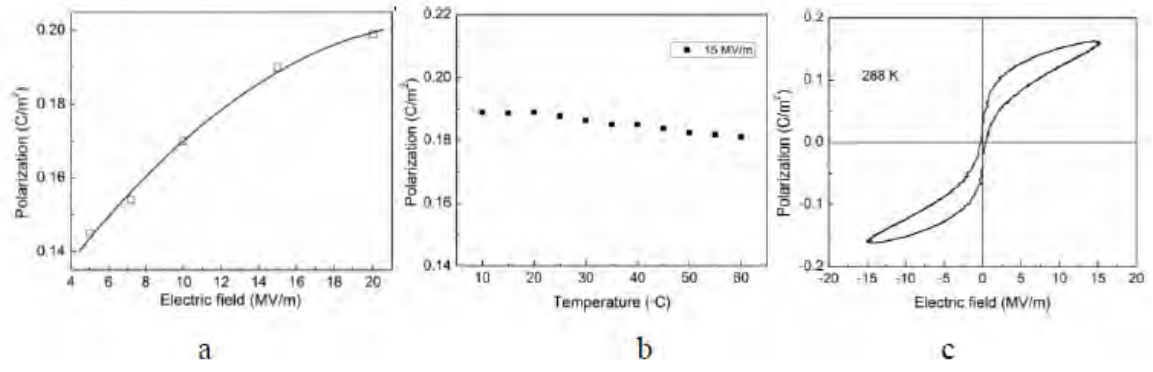

Fig. 14. (a) Polarization as a function of electric field at room temperature; (b) Polarization as a function of temperature under 15 MV/m; (c) The P-E loop measured at 10 Hz at 288 K for BZT x=0.2 thick film .

presented in **Fig. 15**. Such enhancement is likely caused by the stress induced from the substrate

(only two BZT layers are under electric field). The results indicate the potential of much higher ECE exploiting ICP with additional stress variables.

In order to quantify the efficiency of ECE, according to the thermodynamic phenomenological theory, the entropy change ΔS is related to the electric displacement D for the materials with central symmetry, $\Delta S = -\beta D^2/2$, where β is a coefficient. Besides, applying the following equation $-T\Delta S = c\Delta T$ yields the adiabatic temperature change $\Delta T = \beta T D^2/2c$, where c is the specific heat capacity. Apply the data of polarization and ECE of samples, the β values of BZT thick film is shown in **Fig. 15**(c). The value of β is 3.5×10^6 at 11.7 MV/m, which is higher than bulk ceramic (less than 3.0×10^6).

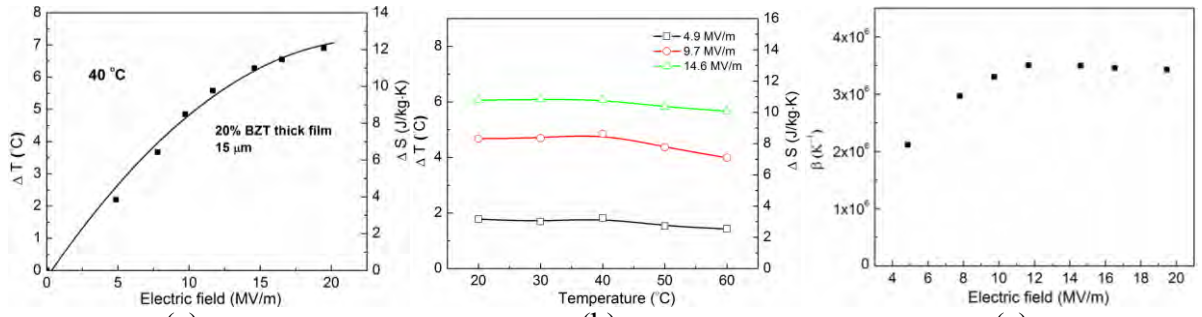

(a) (b) (c)

Fig. 15. (a) ΔT as a function of field measured at 40 C; (b) ΔT as a function of temperature measured at different field, and (c) β vs applied field for BZT x=0.2 thick films.

III. Interfacial effects from the ZrO_2 nanoparticles in the relaxor ferroelectric P(VDF- TrFE-CFE) terpolymers

Composite approach, such as polymer blends and polymer-inorganic nanoparticle composites, is one facile method of tuning polymer properties, and has demonstrated great success in enhancing the dielectric behavior of ferroelectric polymers. Especially, for the polymer-inorganic nanoparticle composites, the interfacial effects may introduce additional polarization process that can result in an improved polarization response and elevated polarization level. From the Landau-Devonshire (L-D) phenomenological theory, the isothermal entropy change ΔS from the ECE is directly proportional to the square of the electric displacement ΔD

$$\Delta S = -1/2\beta (\Delta D)^2 \qquad (7)$$

where β is a coefficient in the L-D theory. Therefore, it may be expected that the ECE can also be enhanced through nanocomposite approach.

In this project, we investigated surface-functionalized ZrO_2 nano-fillers exhibit good compatibility with the polymer matrix, ensuring a uniform distribution of the nano-fillers in the composite films. It was observed that the interfacial effects between the polymer matrix and nano-fillers enhance the polarization response and provide additional entropy changes under electric field. As a consequence, the electrocaloric effect in the composites is enhanced, i.e., the adiabatic temperature change increases to ~120% of that of the neat terpolymer.

The ZrO_2 nanoparticles (~25 nm, Alfa Aesar) was modified by 3-Phosphonopropionic acid (PPA, Sigma Aldrich), which improves the dispersion of nanoparticles in organic solvents and polymer matrix. The ZrO_2 nanoparticle solution was mixed with terpolymer solution (DMF as

the solvent) in a proper ratio and then poured onto a clean glass slide and dried at 50 ^{o}C. After the solvent evaporated, the composite film was peeled off and annealed at 105 ^{o}C for 24h to improve crystallinity and remove the residual solvent. Presented in **Fig. 16** is a SEM image of the nanocomposites with 3 vol% of ZrO_3 nanoparticles, which shows that ZrO_2 nanoparticles are evenly distributed in the polymer matrix without forming large agglomeration. This is distinctively different from the nanocomposites prepared using un-surface modified ZrO_2 nanoparticles. **Fig. 17**(a) presents P-E loops of the terpolymer and its nanocomposites under a uni- polar electric field of 150 MV/m at 10 Hz. The nanocomposites exhibit higher polarization than that of the terpolymer in the field range measured. It should also be noted that the polarization of the nanocomposite at E=0 after one charge/discharge cycle is the same as terpolymer, indicating the enhancement of polarization is intrinsic instead of caused by conduction. The nanocomposite with 1 vol% of ZrO_2 nanoparticles show the strongest polarization enhancement and enhancement gradually reaches saturation, as shown in the insets of **Fig. 17**(a). The nanocomposite with 3 vol% nanoparticles exhibits an induced polarization of 0.069 C/m^2 under 150 MV/m, which is 15% higher than that of neat terpolymer (0.060 C/m^2).

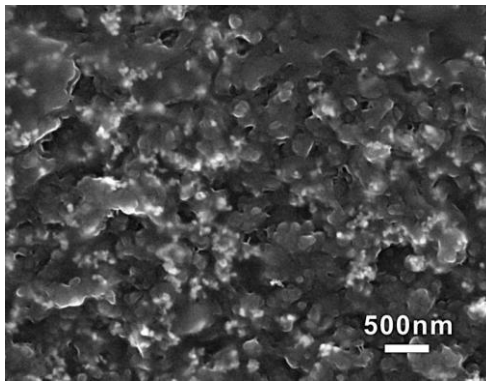

Fig. 16. Cross section SEM image of P(VDF-TrFE-CFE)/ZrO_2

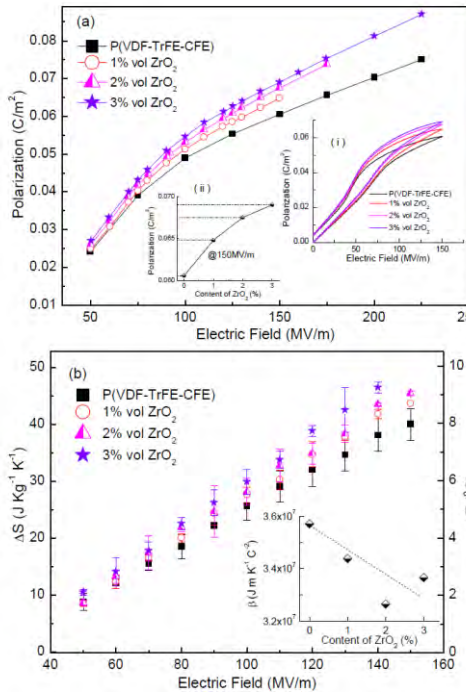

Fig. 17. (a) The variation of polarization measured at different electric fields of nanocomposties with different ZrO_2 content. The insets show the typical unipolar P-E Loops of terpolymer and nanocomposites (i) and variation of maximum polarization with respect to ZrO_2 content (ii). (b) The electric field dependent entropy change (ΔS) and adiabatic temperature change (ΔT) of terpolymer and nanocomposites measured at room temperature.

The direct consequence of the enhanced polarization response is the increase of the electrocaloric effect in the nanocomposites compared with that of the terpolymer. **Fig. 17**(b) compares the isothermal entropy change (ΔS) of the terpolymer and nanocomposites as functions of electric field measured at room temperature. As can be seen, nanocomposites show higher ΔS than that of the neat terpolymer at all electric fields measured, especially at higher electric field. For example, at 140 MV/m, a ΔS ~ 46 J Kg^{-1} K^{-1}, corresponding to a ΔT ~ 9.2 ^{o}C, is induced in the nanocomposite with 3 vol% of nanoparticles, about 20% higher than that of the pure terpolymer (ΔS ~38 J Kg^{-1} K^{-1}, corresponding to a ΔT ~ 7.6 ^{o}C).

Eq. (1) is used to deduce the coefficient β from the experimental data in **Figs. 17**(a) **and 17**(b) and as shown in the inset of **Fig. 17**(b), β thus obtained for the nanocomposites with 0 %, 1 vol%, 2 vol%, and 3

vol%, are 3.57×10^7, 3.44×10^7, 3.27×10^7, and 3.37×10^7 $JmK^{-1}C^{-2}$, respectively. The slightly decrease of β with the nanoparticle content may be attributed to the electrocaloric inactive nature of the ZrO_2 nanofillers. However, the enhanced polarization caused by interface effects suppresses the decrease in β and therefore the resulting ECE in the nanocomposites is still enhanced.

To probe the interfacial effects on the dielectric responses, the dielectric relaxation spectra, especially at relatively low frequencies, were characterized for the composites. **Fig. 18** presents the temperature dependence of the weak field dielectric properties of the terpolymer and its nanocomposites. The broad dielectric constant peaks shift progressively towards higher temperature with frequency, showing typical relaxor characteristics. It is noteworthy that a new dielectric anomaly appears in the dielectric constants of nanocomposite at around 20 ^oC, especially at low frequencies, which is believed to be caused by a low frequency relaxation process due to the heterogeneous nature of the composites. The anomaly was not observed in the terpolymer-ZrO_2 nanocomposites studied earlier in which the nanoparticles were not modified, but observed in the other terpolymer nancomposites with surface-modified nanoparticles. The surface modification allows polymer to wet surfaces of nano fillers and improves the interaction between the nano-fillers and polymer matrix.

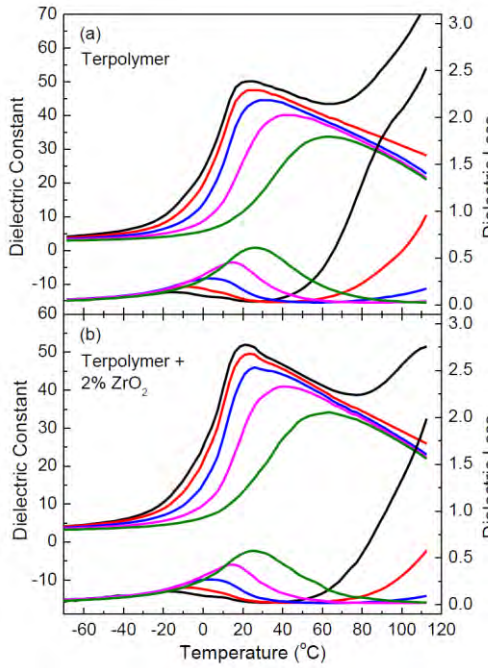

Fig. 18. Temperature dependent dielectric constant and dielectric loss of pure terpolymer (a) and nanocomposites with 2% ZrO_2 nanoparticles at different frequencies (from 100 Hz to 10 MHz).

The superior dielectric and ferroelectric properties of the PVDF based electroactive polymers originate from their crystalline phases. To investigate the influence of the ZrO2 nanoparticles on the crystallization behavior of the polymer matrix, DSC measurements were carried out. **Fig. 19** shows the DSC profiles of the polymers and nanocomposites during the cooling scan. The introduction of the nanoparticles into the polymers raised the crystallization temperature, from ~99 ^oC for terpolymer to ~101 ^oC for the nanocomposite containing 1 vol % ZrO2, indicating the nanoparticles possibly serve as nucleating agent in the crystallization of the polymer matrix. It is noted that the crystallization temperature of the nanocomposites did not show changes as the volume content of ZrO2 nanoparticles increased further. The heat of melting H increased from 23.2 J/g for the terpolymer to 24.1 J/g, 24.8 J/g and 24.6 J/g for the composites with 1 vol%, 2 vol% and 3 vol% ZrO_2, respectively. The heat of melting, which is directly proportional to the crystallity, varied slightly when the nanoparticle loading increased beyond 1 vol%, which suggests that the increased crystallinity

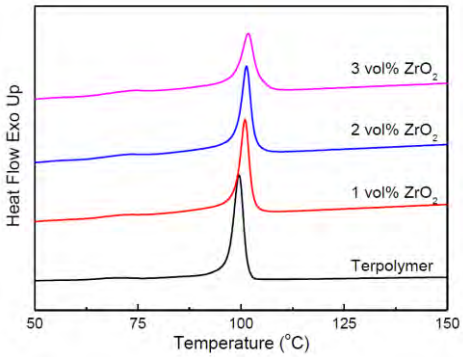

Fig. 19. DSC traces of terpolymer and nanocomposites obtained during the cooling scan.

is not the main reason for the enhanced EC effect observed. For example, assuming the isothermal entropy change ΔS is solely originated from the crystal phase, the neat terpolymer has a ratio of ΔS/ΔH of 1.64. For the composite with 3 vol% ZrO_2, the increase in ΔS from the crystallinity is 40.3 J kg^{-1} K^{-1}, which is much smaller than the observed ΔS = 46 J kg^{-1} K^{-1}, suggesting the interfacial effects cause additional polarization responses which are the major reason for the enhanced ECE observed.

IV. The polymer blends of P(VDF-TrFE-CFE) relaxor with a P(VDF-TrFE) normal ferroelectric have been investigated.

A more than 50% enhancement in the ECE has been achieved in the blends with 10wt% of P(VDF-TrFE) copolymer. We have also started the study of nanocomposites of P(VDF-TrFE-CFE) with inorganic nanoparticles. One objective of these studies is to develop understanding on how these "other" components introduced affect the ferroelectric response, polar-ordering (or randomness), and ECE in the relaxor.

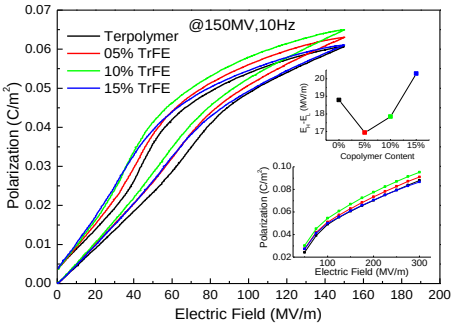

Fig. 20. Unipolar P-E loops of blends with different copolymer wt% at room temperature under an electric field of 150MV/m of 10 Hz. The inset shows (i) The polarization hysteresis of the P-E loops for the blends with different copolymer content and (ii) maximum polarizations of terpolymer and its blends measured at 10 Hz from 50MV/m to 300MV/m.

Fig. 20 presents the polarization behavior of pure terpolymer and its blends under a unipolar 150 MV/m 10 Hz AC field at room temperature. The blends with 5 wt% and 10 wt% copolymer exhibit higher polarization level than that of pure terpolymer. Although for blends with 15wt% copolymer, the enhancement in polarization becomes smaller, the polarization at fields < 150 MV/m is still higher than that of terpolymer. Since blends are relaxor ferroelectric/normal ferroelectric nanocomposites, its polarization response such as hysteresis may change with the copolymer content. Presented in the inset of **Fig. 20** is the maximum polarization hysteresis E_H-E_L at $P_{max}/2$ for the data in **Fig. 20**, where P_{max} is the maximum polarization at 150 MV/m, E_H and E_L are the fields at $P_{max}/2$ in increasing and decreasing the field. As can be seen, E_H-E_L first decreases when 5 wt% copolymer is included, and then increase monotonically with the addition of copolymer. For the blends with 15 wt% of copolymer, the polarization hysteresis is higher than the neat terpolymer. The maximum polarizations of the blends and neat terpolymer measured under different field amplitude from 50 MV/m to 300 MV/m are also summarized in the inset of **Fig. 20**, which show that the polarization of blends with low content of P(VDF-TrFE) are higher than that of pure terpolymer at all electric fields.

Fig. 21(a) present the adiabatic temperature change (ΔT) of the terpolymer and its blends as a function of electric field measured at room temperature. As can be seen, blends show higher ΔT than that of the neat terpolymer at all electric fields measured. For example, at 150 MV/m, a ΔT ~ 8 ^oC is induced in pure terpolymer, while in blends with 10 wt% copolymer a ΔT ~ 10 ^oC is obtained. For blends with 15 wt% of copolymer, ΔT is higher at fields < 100 MV/m and above that ΔT is nearly the same as that of pure terpolymer.

The ΔT as a function of sample temperature under 100 MV/m is shown in **Fig. 21**(b). The ΔT displays a weak temperature variation, which trend is similar to the temperature variation of the dielectric response observed in terpolymer and its blends.

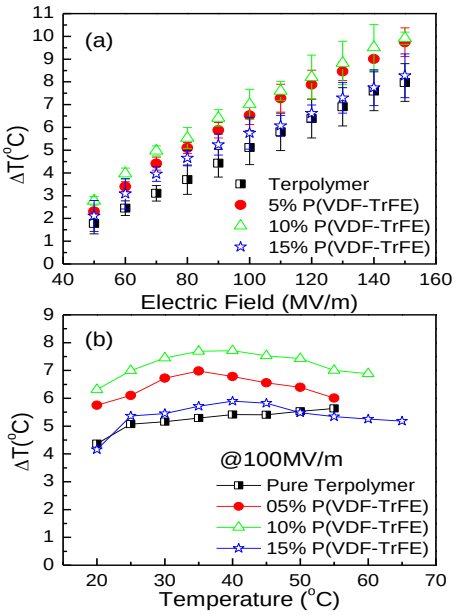

Fig. 21. (a) Adiabatic temperature change as a function of electric field at room temperature. Error bars are indicated. (b) Adiabatic temperature changes as a function of temperature at 100 MV/m.

To examine what contribute to the observed increase in the dielectric and polarization response, DSC and x-ray measurements were carried out. DSC profiles acquired during the first heating process are presented in **Fig. 22**. The relaxor terpolymer does not have FE-PE transition and exhibits a melting peak at 128.3 ºC while the normal ferroelectric P(VDF-TrFE) copolymer displays both a FE-PE transition (65 ºC) and a melting (156.5 ºC), as expected for these polymers. It is interesting to note that while the blended samples exhibit two melting peaks, which correspond to the melting of the terpolymer, around 127 ºC, and that of the copolymer, around 150 ºC, there is no FE-PE transition peak at 65ºC.

The two melting peaks indicate that the two components are not completely miscible. Or, at least crystallization induces phase separation. Nevertheless, the lower melting temperature and the diffused melting peak in the terpolymer components indicates that the copolymer indeed influence the crystalline phases in terpolymer. The total melting heat, and the normalized melting heat of terpolymer component (the actual heat of melting of terpolymer component divided by the weight ratio) are summarized in Table II. The total melting heat (ΔH_m) is increased after addition of copolymer. The normalized heat of melting ($\Delta H_{m(ter)}$) of terpolymer component in the blends is also larger than that of pure terpolymer. The data reveal that the addition of copolymer increases the crystallinity of the blends. As most polarization originates in the crystalline phase, the enhanced crystallinity will lead to larger polarization. The disappearance of the FE-PE transition peak for the copolymer in the blends indicates that the ferroelectric response of the crystalline phase of the copolymer is strongly influenced by the defects, i.e., the bulky CFE (chlorofluoroethylene), in the terpolymer through the interfaces in the blends. The interface couplings with the terpolymer convert the nano-crystallites of the copolymer from a normal ferroelectric to a relaxor ferrolectric. These two effects: increased crystallinity in the blends and conversion of the copolymer from a normal ferroelectric to a relaxor lead to an increased relaxor polarization response and an enhanced ECE. With increased copolymer content to 15 wt% in the blends, this interface effect becomes less effective, as evidenced by an increase in the broad dielectric constant

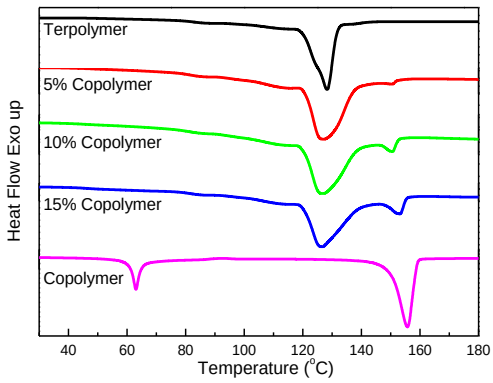

Fig. 22. DSC traces of P(VDF-TrFE-CFE) terpolymer, P(VDF-TrFE) 55/45 copolymer and their blends.

peak towards higher temperature and an increased polarization hysteresis under high electric fields (Fig. 20).

We also proposed to study the ECE and molecular structures in the relaxor P(VDF-TrFE-CTFE) synthesized via the reduction method. *During the first year, we synthesized these polymers and characterized the ECE. It was observed that the ECE of these reduced terpolymers is very small*. Although from the ECE application point of view, the material may not be attractive, it may provide a very interesting material system to understand why the ECE is so small here. In the future of this program, more detailed molecular level studies will be carried out.

TABLE II. Summary of XRD and DSC Data of the Blends

Composition Ter/Co	DSC			XRD	
	T_{m1}, °C	ΔH_m, J/g	Normalized $\Delta H_{m(ter)}$	d, Å	L, nm
100/0	128.3	22.8	22.8	4.86	40.5
95/5	126.8	24.4	24.0	4.87	34.6
90/10	126.7	25.2	25.2	4.86	31.8
85/15	126.6	23.7	23.6	4.87	24.5
0/100	156.5	30.6			

V. Anomalous ECE in normal ferroelectric/relaxor ferroelectric polymer blends.

In general, applying an electric field to a polar dielectric increases dipole ordering, as illustrated in **Fig. 23A**. This ordering reduces the dipolar entropy of the dielectric. Under an adiabatic condition, this entropy reduction ΔS leads to a heat release and thus a temperature increase ΔT (**Fig. 23B**). As the field is removed, the dipoles return to their less ordered state and the dielectric absorbs heat, shown as the blue peak in **Fig. 23B**. The recent discovery of dielectric materials with giant ECE has stimulated great interest in developing cooling technologies that are environmentally friendly and have the potential to achieve higher efficiency compared with the century-old, vapor compression based cooling technology (2-13). Analogous to the inverse magnetocaloric effect reported earlier (14), the negative (or inverse) ECE (N-ECE) has also been observed in ferroelectric materials in which an applied electric field causes a reduction of dipole ordering, generating cooling, and the removal of the electric field causes heating in the dielectric material (see illustration in **Fig. 23C**) (15-18).

Now if one can design a polar-dielectric in which, at the poled state, the dipoles are in an ordered state with relatively large remnant polarization, and the ordered state will be converted to a dipole random state when subjected to a de-poling field, absorbing heat, then one can overcome the limitations of conventional polar-dielectrics. Because this de-poling process involves a transition from a dipole ordered to a dipole random state, the N-ECE can be much larger than that in a normal ferroelectric. Moreover, upon reducing the de-poling field to zero, the material can still retain its dipole disordered state, which will remove the subsequent heating peak as observed in the normal ferroelectric polymers (**Fig. 23D**). Here, we show that such a polar-dielectric material can be realized in hybrid normal ferroelectric/relaxor ferroelectric polymer blends, in which the coupling between the two constituents (see their D-E loops in **Fig. 24A**) stabilizes the polar-ordering in the relaxor ferroelectric region in the poled state, see **Fig. 24C** and **Fig. 24D** of the temperature-dependent dielectric constant and D-E loop of the hybrid, while in the de-poled state,

the dipolar random state can be retained by the relaxor terpolymer in the blends after the de-poling field is reduced to zero.

The weight ratio between the two polymers is 50/50, displaying a lower remnant polarization P_r and coercive field E_{coer} than those of the normal ferroelectric constituent, which is understandable because of the presence of 50 wt% of relaxor terpolymer in the blends. Here we denote this hybrid as TC50-65/35, where T and C denote terpolymer and copolymer, respectively: 50 refers to the wt% of the terpolymer in the blends; and 65/35 refers to composition of the copolymer. Since the densities of the two polymers are nearly the same, the volume ratio of the two polymers in the hybrid is nearly the same as the weight ratio.

A comparison of **Fig. 24**A and **Fig. 24**D reveals that TC50-65/35 blends have a P_r=0.044 C/m^2, which is not far from that of the copolymer (P_r=0.054 C/m^2). Considering that the copolymer content is 50 wt% in the blends, the observed large ratio of P_r(blends)/P_r(copolymer) suggests that the normal ferroelectric copolymer induces polarization in the terpolymer regions in the poled state, resulting in a large P_r. The results here are confirmed by a phase field simulation, presented in **Fig. 25**, which shows that the local fields of the copolymer constituent in the poled state induce polarization in the terpolymer regions in the blends. Differential scanning calorimetry was carried out to characterize the phase behavior of the blends. The results are presented in **Fig. 26** for the blends of TC50-65/35, the terpolymer, and the 65/35 mol% copolymer, respectively. The blends display two distinctive melting peaks, corresponding to those of the copolymer and terpolymer, and a FE-PE transition peak, due to the copolymer, albeit the FE-PE transition peak is broader in the blends compared with the copolymer, owing to the coupling of the copolymer to the terpolymer.

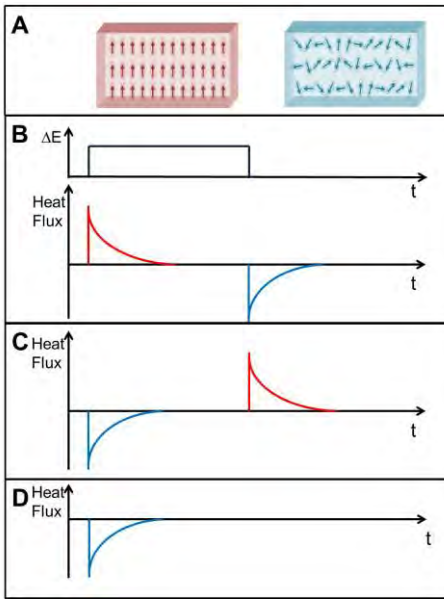

Fig. 23. Schematics of positive/negative electrocaloric effect (ECE) and proposed anomalous ECE (A-ECE). (A) Dielectric material in dipole ordered and disordered state. (B) Heat flux signal in normal ECE case. (C) N-ECE case. (D) A-ECE case.

In such a hybrid, applying a de-poling field will transition the material to a dipole random state, yielding a large N-ECE, as shown in **Fig. 24E**, where the TC50-65/35 blends display an isothermal entropy change ΔS = 11.5 J/(kgK) (ΔT = -2.1 K) when the de-poling field = E_{coer}, the coercive field, indicated by the arrow in the D-E loop in Fig. 2D. More interestingly, the hybrid does not show a subsequent heating peak when the de-poling field is reduced to zero, yielding a new class of EC material which exhibits a large N-ECE without the subsequent heating peak under an electric pulse, i.e., the A-ECE.

Fig. 24E presents the A-ECE for the hybrid blends with different P(VDF-TrFE) copolymer compositions, among which the TC50-65/35 blends exhibit the largest A-ECE. The TC50-55/45 blends show a smaller A-ECE, due to their low dipole ordering in the poled state (see the D-E loop in **Fig. 27A**). On the other hand, TC50-75/25 exhibits an N-ECE as appears in normal ferroelectrics, i.e., a small cooling peak (ΔS = 1.8 J/(kgK)) as the de-poling field is applied, followed by a weak heating peak (ΔS < 1 J/(kgK)) upon the removal of the de-poling field. This is

also consistent with the D-E loop of TC50-75/25 shown in **Fig. 27B**. The D-E loops in **Fig. 27** and **Fig. 24** show that the blends with 55/45 mol% copolymer display a very low remnant polarization, i.e., P_r of the blends is less than 50% of P_r of the 55/45 mol% copolymer, indicating that in the TC50-55/45 blends, the weak ferroelectric ordering in the 55/45 mol% copolymer is not strong enough to stabilize the polarization in the terpolymer in the poled state, resulting in a weak polar-ordering in the poled state and a smaller A-ECE, compared with that of TC50-65/35. On the other hand, the blends with 75/25 mol% copolymer (TC50-75/25) display a D-E loop not much different from that of the neat copolymer and hence display an N-ECE.

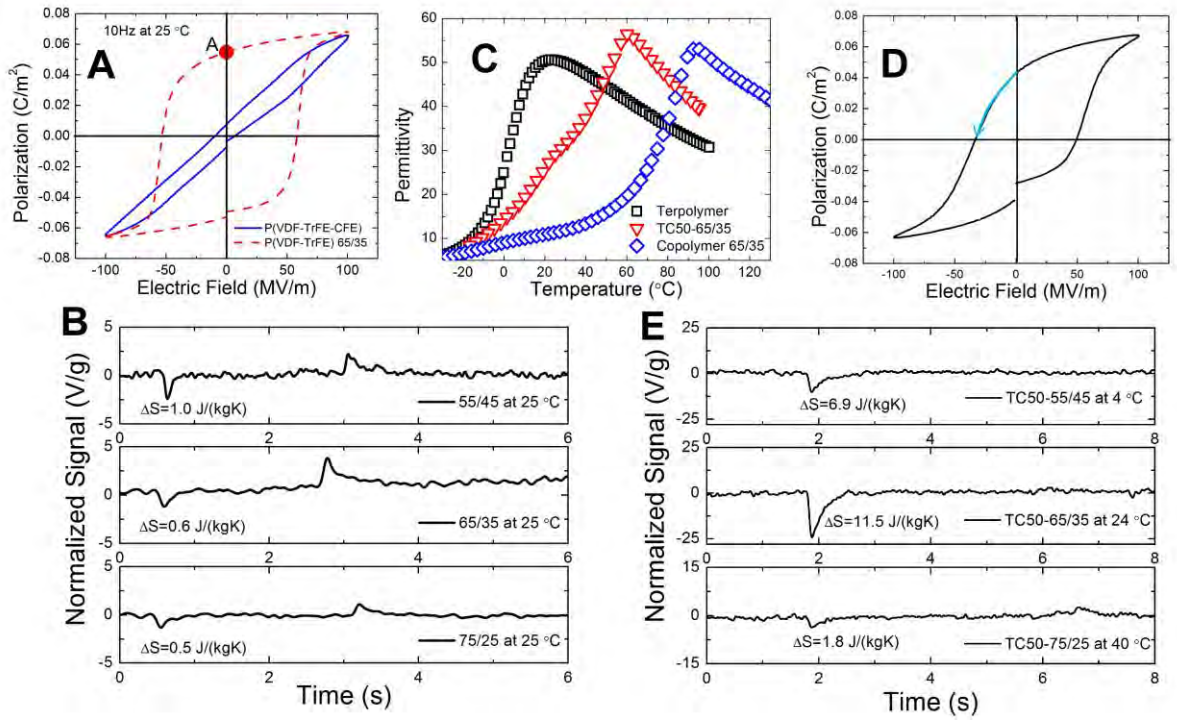

Fig. 24. Comparison of dielectric properties and direct-measured ECE signals between neat copolymers and blends. (**A**) The D-E hysteresis loops for the normal ferroelectric 65/35 mol% copolymer and the relaxor P(VDF-TrFE-CFE) terpolymer. Applying a de-poling field in the copolymer generates an N-ECE. (**B**) The N-ECE for the copolymers of 55/45 mol%, 65/35 mol%, and 75/25 mol%. ΔS from the cooling peak is shown in the figure. (**C**) The dielectric constant vs. temperature measured at 1 kHz for the 65/35 mol% copolymer, the terpolymer, and the TC50-65/35 blend. (**D**) The D-E loop of the blends TC50-65/35, where the arrow indicates the de-poling field = E_{coer}, the coercive field. (**E**) The anomalous ECE in TC50-55/45 and TC50-65/35, and the N-ECE in TC50-75/25.

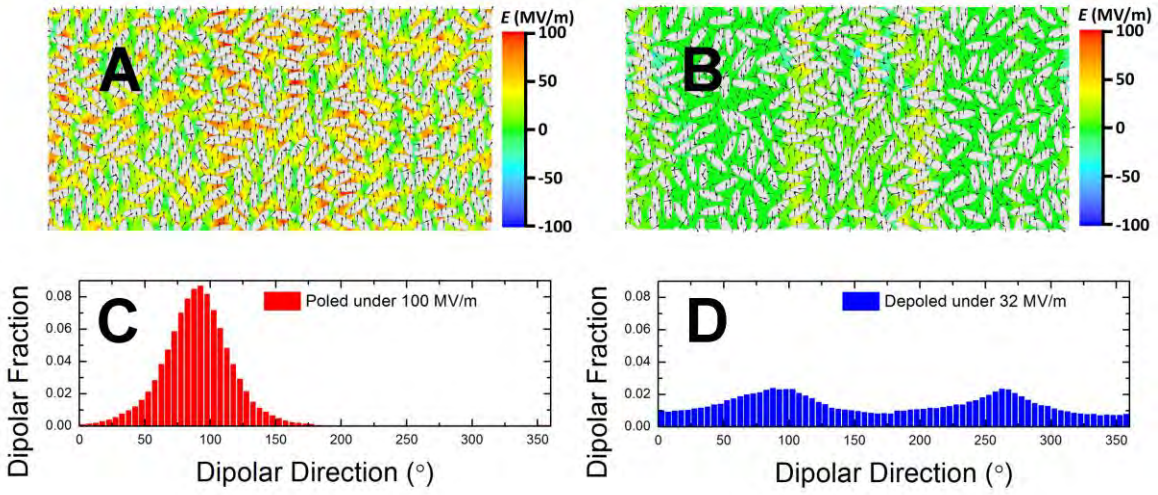

Fig. 25. Phase field simulation results, (**A)**, (**B)**, (**C)**, and (**D)**. The dipolar direction distribution in such a hybrid was simulated (Fig. 25**A** for the poled state and 25**B** for the de-poled state). The fractions of dipolar orientations with respect to the original poling directions (orientation = 90º) deduced from Figs. 25**A** and 25**B** are presented in Figs. 25**C** and 25**D** for the poled state and the de-poled state, respectively. The strong ordering provided by the copolymer induces an internal electric field and aligns the dipoles in the ferroelectric relaxor terpolymer matrix (Fig. 25**A**); thus the dipolar directions are distributed around 90 degrees (Fig. 25**C**), the poling field direction. After being de-poled with a field of 32 MV/m, the normal ferroelectric component is de-poled, and the relaxor component does not show polarization. In addition, the dipolar randomness can be stabilized (Fig. 25**B** and Fig. 25**D**) owing to the presence of ferroelectric relaxor teropolymers.

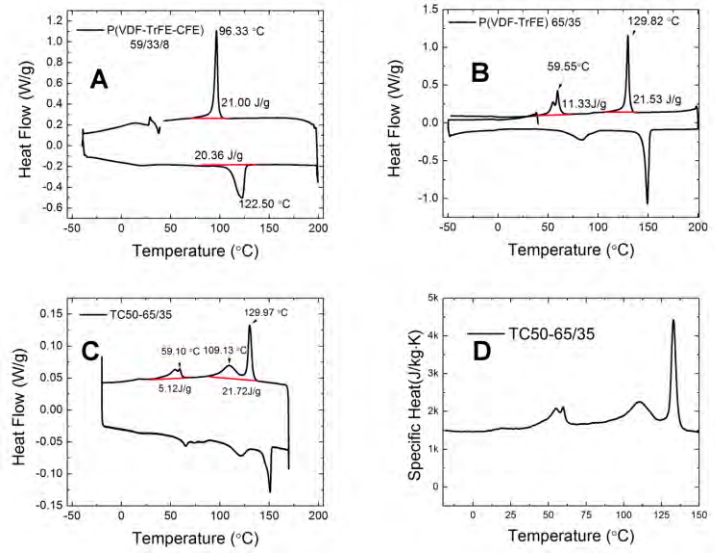

Fig. 26. (**A**) DSC scans taken during heating and cooling runs, showing the melting of the copolymer (~ 151 ºC), the terpolymer (~ 120 ºC), and the FE-PE transition of the copolymer. (**B**) Copolymer DSC scans taken during heating and cooling runs. (**C**) Terpolymer DSC scans taken during heating and cooling runs. (**D**) Specific heat data measured during cooling using a modulated DSC.

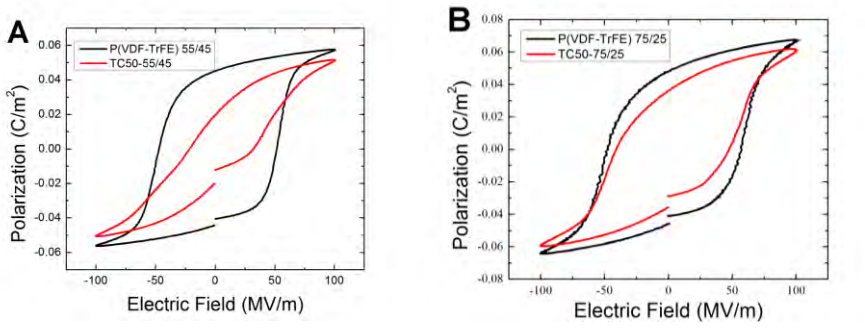

Fig. 27. Comparison of the D-E loops: (**A**) 55/45 mol% copolymer and TC50-55/45 blends, and (**B**) 75/25 mol% copolymer and TC50-75/25 blends.

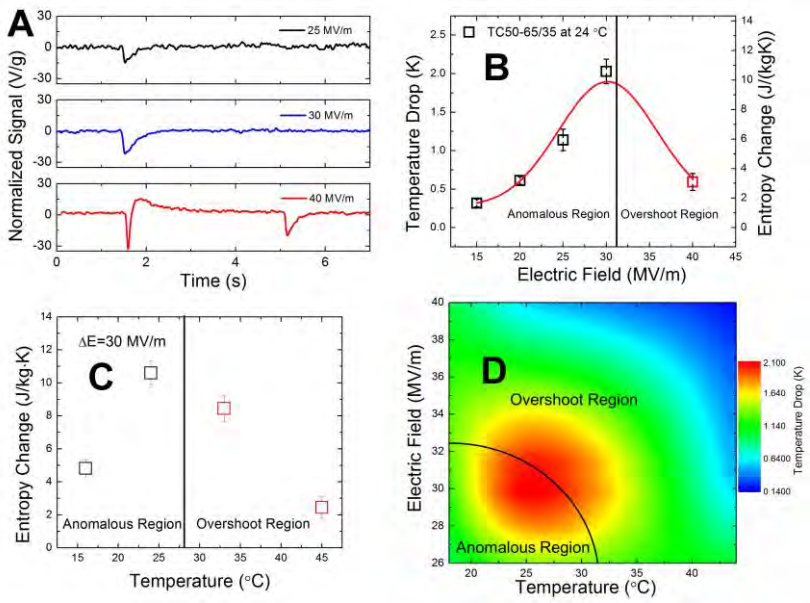

Fig. 28. Temperature and electric field dependences of A-ECE. (**A**) Evolution of the A-ECE vs. de-poling field strength for CT50-65/35, from the A-ECE at $E < E_{coer}$ to the field overshoot region (40 MV/m) where the applied field first induces a cooling peak and then, immediately, a heating peak as the field exceeds E_{coer}. As a result of the poling under E=40 MV/m, the blends also show a heating peak upon reducing the field to zero. (**B**) ΔS and ΔT vs. the applied de-poling field at 24 ºC, showing the evolution from the A-ECE to the field overshoot ECE. The ΔS for the field overshoot ECE is the combination of the cooling and heating peaks at the application of the de-poling field. (**C**) ΔS vs. temperature under 30 MV/m. Increasing temperature causes a reduction of E_{coer} and hence a crossover from the A-ECE to the field overshoot when measured under a fixed field. (**D**) 2-D plot (temperature and de-poling field) of the A-ECE and field overshoot regions for the TC50-65/35 blends. The black curve indicates the boundary between the A-ECE and field overshoot ECE.

Fig. 28 presents the dependence of A-ECE on the de-poling field. The data shows that the A-ECE increases with the de-poling (or "negative") field till it reaches the coercive field E_{coer}. As the "negative" field increases beyond E_{coer} (field overshoot), the blends will be poled to the negative direction, generating a heating peak due to the increased ordering, as shown in **Fig. 28A**

for the de-poling field = 40 MV/m. That is, as the de-poling field is applied, the blends will generate cooling first and then heating as the field is further increased to higher than E_{coer}. After the field becomes > E_{coer}, the polarization of the blend is poled to the negative direction (polarization reverse) and hence shows a positive ECE, i.e., a cooling peak as the field is removed, as shown in experimental data in **Fig. 28A** for the de-poling field = 40 MV/m. **Fig. 28B** summarizes this field dependence of the A-ECE as well as the conversion to the positive ECE at de-poling fields > E_{coer}, i.e., the field overshoot region, for the TC50-65/35 blends. An A-ECE of ΔS=11.5 J/(kgK), which corresponds to ΔT=-2.1K temperature drop, is observed when the de-poling field = E_{coer}, which is 30 MV/m.

For ferroelectric materials, E_{coer} changes with temperature, and hence the electrocaloric response will change with temperature under a given applied de-poling field. **Fig. 28C** presents the A-ECE vs. temperature for TC50-65/35 under the de-poling field of 30 MV/m. At temperatures below 28 ^{o}C the blends show the A-ECE, and above that temperature, a field overshoot ECE behavior is observed because E_{coer} < 30 MV/m at temperatures higher than 28 ^{o}C. A 2-dimensional plot of the evolution of A-ECE as a function of the de-poling field and temperature is presented in **Fig. 28D**.

The evolution of the EC response under the de-poling field = E_{coer}, from the N-ECE of the neat copolymer (**Fig. 24B**) to the A-ECE (**Fig. 24E**) of the TCx-65/35 blends with the terpolymer content *x*, was investigated and presented in **Fig. 29** As the terpolymer content *x* in the blends increases beyond zero, the cooling peak (ΔS) increases while the heating peak decreases. At *x*=50 wt% (TC50-65/35), the cooling peak reaches the maximum while the heating peak disappears. Beyond x = 50 wt%, the blends exhibit the A-ECE. Because E_{coer} decreases (and hence the applied de-poling field also decreases) with *x*, the A-ECE (cooling peak) becomes smaller with *x* for *x* > 50 wt%. For TC75-65/35, the cooling peak becomes smaller than the instrument resolution. The "blends" with *x*=100 wt% are the pure terpolymers, which have E_{coer} = 0 at room temperature and exhibit giant positive ECEs (3,7).

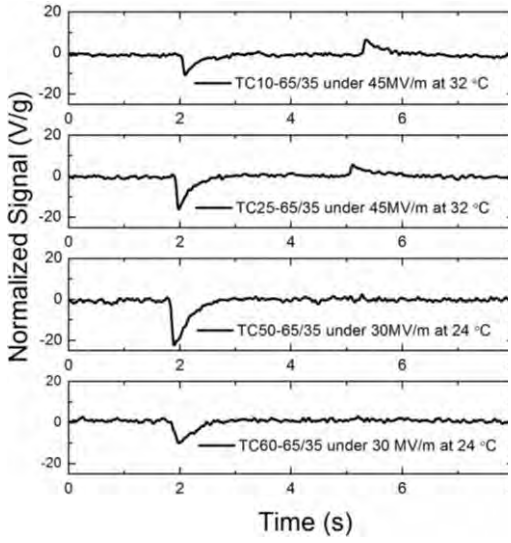

Fig. 29. The evolution of the ECE vs. the terpolymer content, *x*, in the blends of TC*x*-65/35 for the de-poling field = E_{coer}. With increased *x*, the blends evolve from the N-ECE to the A-ECE, i.e., the cooling peak (ΔS) of the N-ECE increases and the heating peak decreases till TC50-65/35, at which point no heating peak is detected. For *x*>50 wt%, the blends show the A-ECE, and now the cooling peak decreases with *x*. The blends TC50-65/35 show the largest ΔS of the cooling peak. Measurements were carried out at different temperatures for different compositions so that the ΔS of the cooling peak is the largest for a given composition.

In conclusion, we report an anomalous EC effect in a hybrid normal ferroelectric/relaxor ferroelectric polymer blend that is produced by the mesoscale dipolar interactions between the two components. The normal ferroelectric component induces dipole ordering in the relaxor polymer in the poled state, which can be switched to a de-poled state

by an external field; when the de-poling field is removed, this de-poled state can be maintained by the relaxor component. This work paves a way to produce anomalous, large EC effect through engineering mesoscale inhomogeneous dipolar interactions, and thus could lead to many device applications. These devices would absorb heat from the surrounding without subsequent heat release to the surrounding.

Other Metrics: A start-up company has formed (Nascent Devices LLC) to transition these research results to commercial market.

Publications:

- Xiaoshi Qian, Tiannan Yang, Tian Zhang, Long-Qing Chen and Q. M. Zhang, Anomalous Electrocaloric Effect. Submitted to *Adv. Mater.* (2015).
- S. Pamir Alpay, Joseph Mantese, Susan Trolier-McKinstry, Q. M. Zhang, Roger W. Whatmore, Next Generation Electrocaloric and Pyroelectric Materials for Solid State Electrothermal Interconversion. *MRS Bulletin* 39, 1099 (Dec. 2014) (Invited review article).
- Xiao-Shi Qian, Hui-jian Ye, Ying-Tang Zhang, Haiming Gu, Xinyu Li, C. Randell, and Q. M. Zhang. Giant Electrocaloric Response in Modified $BaTiO_3$ Ceramics Over A Broad Temperature Range. *Adv. Funct. Mater*. 24, 1300, (2014) (featured in backcover image of the vol. 25 issue).
- G. Casar, X. Li, Q. M. Zhang, and V. Bobnar, Influencing dielectric properties of relaxor polymer by blending PVDF-TrFE-based terpolymer with a ferroelectric copolymer. *J. Appl. Phys.* 115, 104101 (2014).
- Hui-Jian Ye, Xiao-Shi Qian, Dae-Yong Jeong, Shujun Zhang, Yue Zhou, Wen-Zhu Shao, Liang Zhen, and Q. M. Zhang. Giant electrocaloric effect in $BaZr_{0.2}Ti_{0.8}O_3$ thick film. *Appl. Phys. Lett.* 105, 152908 (2014).
- Xinyu Li, Sheng-Guo Lu, Xiang-Zhong Chen, Haiming Gu, Xiaoshi Qian, Q. M. Zhang. Electrocaloric and Pyroelectric Materials, *J. Materials Chemistry* C1, 23 (Feature Article) (2013).
- Lianyun Yang, Xinyu Li, Elshad Allahyarov, Philip L. Taylor, Q. M. Zhang, and Lei Zhu. Novel Polymer Ferroelectric Behavior via Crystal Isomorphism and the Nanoconfinement Effect. *Polymer*, *54*, 1709-1728 (2013). (feature article).
- Xiang-Zhong Chen, Xinyu Li, Xiao-Shi Qian, Shan Wu, Sheng-Guo. Lu, Hai-Ming Gu, Minren Lin, Qun-Dong Shen, and Q. M. Zhang. A polymer blend approach to tailor the ferroelectric responses in P(VDF-TrFE) based copolymers. *Polymer*, 54, 2373 (2013).
- Xiang-zhong Chen, Xinyu Li, Xiao-shi Qian, Shan Wu, Haiming Gu, Minren Lin, Qun-dong Shen, and Q. M. Zhang. A nanocomposite approach to tailor electrocaloric effect in ferroelectric polymer. *Polymer*, 54, 5299 (2013).
- Xiang-Zhong Chen, Xiao-Shi Qian, Xinyu Li, S. G. Lu, Haiming Gu, Minren Lin, Qun-Dong Shen, and Q. M. Zhang. Enhanced electrocaloric effect in P(VDF-TrFE)-based terpolymer/copolymer blends. *Appl. Phys. Lett*. 100, 222902 (2012).
- Z. K. Liu and Q. M. Zhang. Maximizing the Number of Coexisting Phases Near Invariant Critical Points For Giant Electrocaloric and Electromechanical Responses in Ferroelectrics. *Appl. Phys. Lett*. 101, 082904 (2012).
- R. Su, J. K. Tseng, M. S. Lu, M. Lin, Q. Fu, Q. M. Zhang, and L. Zhu, L. Ferroelectric behavior in the high temperature paraelectric phase in a poly(vinylidene fluoride-*co*-trifluoroethylene) random copolymer. *Polymer*. 53, 728-739 (2012).

Books and Chapters in Books:

- *Electrocaloric Polymers*, Xinyu Li, Sheng-Guo Lu, Xiaoshi Qian, Minren Lin, and Q. M. Zhang. Chapter 5 in *Electrocaloric Materials: New Generation of Coolers*. Tatiana Correia and Qi Zhang, Ed. Springer (2014).

Presentations:

- Q. M. Zhang, Recent Advances in Electrocaloric Materials and Devices, Inha University, S. Korea (Aug. 2013) (Invited)
- Q. M. Zhang, Electroactive Polymers and Nanocomposites, The 7th World Congress on BAMN, Jeju, S. Korea (Aug. 2013). (Invited Keynote)
- Q. M. Zhang, Electroactive Polymers and Related Devices, CAU (Christian-Albrechts-University, Kiel, Germany (Sept. 2013) (Invited)
- Q. M. Zhang, Dielectrics with Large Electrocaloric Effect And Related Cooling Devices, European Conf. on Mater&Tech for Sustainable Growth, Bled, Slovenia (Sept. 2013). (Invited)
- Q. M. Zhang, Beyond the polarization responses in normal ferroelectric polymers – some amazing properties of relaxor ferroelectric polymers. Beijing University of Science and Technology, Beijing, China (January 2014). (Invited)
- Q. M. Zhang, and Xiaoshi Qian, Designing electrocaloric materials, Annual meeting of Center for Dielectric and Piezoelectric Study, State College, PA (May 2014). (Invited)
- Xiaoshi Qian, H. Gu, X. Li, and Q. M. Zhang, Simulation and Device Demonstration of High Performance Chip-Scale Cooling Device based on Giant Electrocaloric Effect Dielectrics, IEEE ISAF meeting, State College, PA (May 2014).
- Q. M. Zhang, Self-assembled multifunctional nanocomposites with large electroactive responses. EueoEAP 2014, Linkopin, Sweden (June 10-11, 2014). (Invited plenary)
- Q. M. Zhang, Designing dielectric materials with giant electrocaloric effect. German SPP 1599 Convention, TU Dresden, Germany (June 22-25, 2014). (Invited).

Honors and Awards:

- Xiaoshi Qian has received Dr. Nirmal K. Bose Dissertation Excellence Award in May 2014 from the Electrical Engineering Department of Penn State.